Simulation and modeling of Rare earth ion based quantum gate operations

Author:
Samuel Bengtsson

Supervisors:
Dr. Peter Samuelsson
Prof. Stefan Kröll

December 13, 2012

Abstract

Quantum gate operations and dipole-dipole interactions are modeled by placing doped rare-earth ions in an Yttrium ortho silicate crystal. The time dependent Schrödinger equation is also solved for different cases where Europium and Praseodymium are exposed to light pulses carrying operations on them. Both a three level Hamiltonian and a six level Hamiltonian is used. Through different simulations and models are the prerequisites for functioning quantum gate operations on rare earth ions studied.

Populärvetenskaplig sammanfattning

I och med samhällets utveckling växer mängden information lavinartat. Med all information kommer vikten av att hitta just den relevanta information som du är ute efter att växa. Som det är nu så kan vanliga datorer klara det på överkomlig tid men i framtiden kommer de inte kunna söka igenom all information på rimlig tid. Något som däremot verkar kunna klara just det och som är väldigt bra på att söka igenom stora mängder med information tros vara kvantdatorer.

Kvantdatorer är fortfarande framför allt ett teoretiskt koncept och man söker efter bästa sättet att förverkliga teorin i praktiken. För ett av sätten, där man har fria joner som är fångade i ett magnetfält, har man lyckats koppla ihop 8 joner till ett system som kan utföra vissa elementära operationer. I Lund så jobbar man med ett fysikaliskt system där sällsynta jordartsjoner sitter i en kristall och laserpulser används för att påverka jonerna på ett kontrollerat sätt.

Med tanke på att det tar flera veckor eller månader att ställa upp ett experiment är det viktigt att man gör ett teoretiskt förarbete, dels för att spara tid och för att vissa effekter ska kunna förstås och förklaras. Därför har denna rapport kommit till för att göra en modell för systemet och för att simulera vad som händer med joner när olika ljuspulser sänds in och sedan analysera resultaten. Målet är att öka kunskapen om detta sätt att förverkliga teorin och så komma ett steg närmare en fungerande kvantdator.

Contents

1   Introduction

As with all great projects the question "why?" is more interesting than "how?" so to better understand the flow of things and have a mental starting point it is indeed worth taking the time to ask. The question does have many answers, true, but one of the fundamental ones for me must be the thirst to understand and develop a new technology. Why else would anyone dedicate their life and youth to live in a dark cellar and shoot lasers at a crystal? Even so, the answer could equally well be "Why not?" and so we find ourselves in a world where quantum computers are slowly crawling into existence.

The first step in doing any quantum computations is to make some quantum gate operations and so this work finds its place in the wheel of time. Firstly is a foundation presented with the basic idea of the quantum computer and quantum gates and similar basic information that is needed to understand the rest of the thesis. Following that chapter is a chapter where the hands-on crystal and ions are presented that are used in this type of quantum operations and through which the steady-state of the system is studied. Describing how the system is evolved in time through solving the time dependent Schrödinger equation is the last step before the results from the different simulations that were made are presented.

The question that the results are going to answer is how the system should be constructed to get the highest probability to succeed with a quantum gate operation. That includes the pulses that are sent into the system and the doping atoms and doping concentration.

2   Quantum computers

2.1   General description

What, then, are "quantum computers"? To understand we compare a quantum computer with a normal personal computer. The difference begins already in the hardware. In the personal computer (PC), information is handled with bits in ones and zeros. This is realized in the Complementary Metal Oxide Semiconductor (CMOS) technology by having different voltages for the one (e.g. 3V) and zero (0V). Using this system the data is moved, processed and stored a billion times each second. In a quantum computer the information can be stored in states in the atom and the smallest information unit is called qubit. An electron belonging to an atom can be in different states but at the end of the day the electrons are occupying all the lowest energy states. Say that we only have two states and one electron, a so called two level system, then it is possible to excite the electron from the lower state to the upper by sending in a photon with the exact right energy corresponding to the energy difference between the states. According to quantum physics the state for the electron can be written as

$$|\psi\rangle = c_0 |0\rangle + c_1 |1\rangle \qquad c_i \in \mathbb{C} \tag{1}$$

where $|\psi\rangle$ describes the total state of the electron and $|c_0|^2 + |c_1|^2 = 1$ which corresponds to the probability to find the electron in the system. This means that the electron can be in a superposition of the eigenstates. Quantum mechanics

teach us however that as soon as the total state is measured it will collapse into one of the eigenstates $|0\rangle$ or $|1\rangle$ with the probability $|c_0|^2$ and $|c_1|^2$.

Another quantum phenomena that is used in quantum computation is entanglement. Entanglement is when two or more ions are in a superposition and the collapse of one ion into a state decides the state of the other ion and is thus a collapse of the whole system. Another way to see it is that the wave function cannot be written as a product state of the wave functions of the individual ions. An example is a Bell state which is defined as

$$|\beta_{00}\rangle = \frac{|00\rangle + |11\rangle}{\sqrt{2}} \tag{2}$$

where the notation $|00\rangle$ describes a wave function where both qubits are in basis state $|0\rangle$. The two qubits will with certainty after the collapse have the same value, even though that value is not decided.

2.2 Bloch sphere

When faced with visualizing a superposition between two states a Bloch sphere becomes handy. For normalized wave functions ψ such as in equation 1 the vector representing the wavefunction points to a point on a sphere with radius one. The poles of the sphere represent when the probability is one to be in one of the states. Thus if the vector is anywhere else on the sphere means that there is a probability to be in either state. As an example is the probability at the equator of the sphere, when $z = 0$, equal to be in the two states. The position in the x-y plane corresponds to the phase between the two states where x is the real axis and y is the imaginary. The vectors and the outlines of the sphere are shown in figure 1.
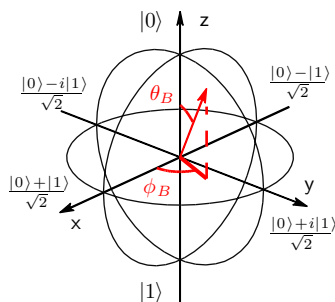
Figure 1: the Bloch sphere [13]

2.3 Gates

To do operations on the qubits different gates are used that change the states of the qubits. The simplest gate is the NOT gate where the probability in $|0\rangle$ and $|1\rangle$ are switched. Another commonly used gate is the Hadamard gate which with the bloch sphere picture, figure 1, shifts the superposition $\frac{\pi}{2}$ around the

5

y-axis and π around the x-axis. This means that from a qubit in the groundstate we get a superposition

$$U_{Hadamard} |0\rangle = \frac{|0\rangle + |1\rangle}{\sqrt{2}} \qquad (3)$$

A third gate that is needed is the controlled NOT (CNOT). The CNOT gate involves two qubits as opposed to the other two gates than only work on one qubit. One of the qubits is the control qubit on which nothing is changed. The other qubit is the target where a NOT gate might or might not be applied. This depends on whether the control qubit is in $|1\rangle$ or not. Using this gate a Bell state can easily be made by having the control ion in $\frac{|0\rangle + |1\rangle}{\sqrt{2}}$ and the target in $|0\rangle$.

2.4 Algorithms

Suppose two qubits are in a superposition $|\psi\rangle = \frac{(|0\rangle + |1\rangle)}{\sqrt{2}} \cdot \frac{(|0\rangle + |1\rangle)}{\sqrt{2}}$ where the first term is the first qubit and the second term the second qubit which can be rewritten as $|\psi\rangle = (|00\rangle + |01\rangle + |10\rangle + |11\rangle)/2$. This superposition holds all the values those two bits can hold and as the careful reader notice they are not entangled. This is scalable, meaning that with eight qubits a superposition state can be created where all the possible 256 values are equally weighted simply by changing all the qubits into the superposition $|\psi\rangle = \frac{(|0\rangle + |1\rangle)}{\sqrt{2}}$ and so on with even more qubits. If a operation is done on the wave function with equal probability to have all values finding the needle in the haystack is intuitively easier since that value is also subjected to the operation. Thus it does not come as a big surprise that quantum computers are especially good at searching through loads of data. Using this approach specific values such as the factors of a large number can be found faster than doing it the classical way. Since quantum computers are so different from normal computers special algorithms are needed like the Deutsch-Jozsa algorithm and the Shor factoring algorithm [14].

In this thesis the Deutsch-Jozsa algorithm was simulated. The algorithm is more of a fundamental quantum computing algorithm and not really good for anything but demonstrating that a quantum algorithm can be exponentially faster than any classical algorithm when searching for the answer on a question. What it does is to check if a function is balanced or not. This means, if the function returns the same result for all input values or if the results are balanced such that half the input values return $|1\rangle$ and the other half return $|0\rangle$. One such function that is unbalanced is a function that is independent of the input values, and a balanced function can return the value of one qubit. In a classical way this question is answered by checking the function for half the input values plus one. Thus the number of operations is proportional to the number of input values. In the Deutsch-Jozsa algorithm the input values grow exponentially with the number of qubits. The additional time needed when doubling the input values for classical approach is roughly the double while for the quantum algorithm it is the time to target one qubit with pulses. A schematic sketch for the Deutsch-Jozsa algorithm is shown in figure 2. If the qubits measured after the algorithm are all in $|0\rangle$ then the function is unbalanced.
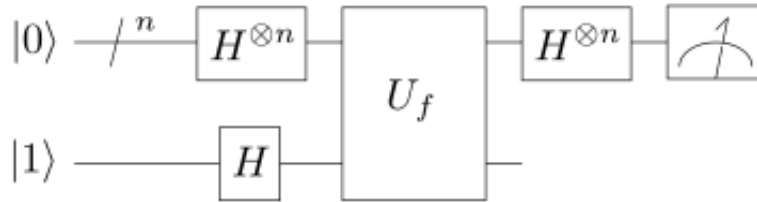
Figure 2: A schematic picture of the Deutsch-Jozsa algorithm. The top line is the query register where the input qubits are. The bottom line is the answer register where one qubit is prepared into state $|1\rangle$. On all of them are Hadamard gates (H) applied which creates superpositions with equal probability of being in $|0\rangle$ and $|1\rangle$. In U_f is the function targeted on the answer qubit with input from the query register. After the operation is Hadamard gates once again applied to the query qubits and the values are measured on them.

2.5 Fidelity

After an operation has been made on a system the final wave function can be compared to the desired wave function to evaluate how successful the operation was. This is called the fidelity of the operation and is defined as $|\langle \psi_{final}|\psi_{ideal}\rangle|$. The desired value which is reached for is a fidelity of 99% or better.

2.6 The idea of rare earth ions

There are different ways to realize the quantum computer. One way is by using rare earth ions doped in a crystal. In that system can different states be used as data states. The crucial property is the coherence times of the states since the information need to be left unchanged long enough for several operations to take place. In rare earth ions such states with long coherence times exist. When filling the electron shells the 5s and 5p shell are filled before the 4f shell even though 4f is closer to the core [16]. The half filled shell for rare earth ions is exactly that 4f shell which means that an excitation within that shell is protected from external interferences due to those outer lying filled states which results in those long coherence times. In this shell the different states depend on the total angular momentum from the 4f electrons. As an example the Europium state have six electrons in the 4f shell and due to fine structure splitting the ground state is $^7F_0$. This state with L=3 and J=0 is split into three states because of the hyperfine interaction between the nucleus and the electrons. From these states are chosen a $|0\rangle$, $|1\rangle$ and $|aux\rangle$ where the auxiliary state doesn't contain any data but works as a storage location. From this group of states the transition up to the fine structure split $^5D_0$ is an optical transition, that is within the optical range of frequencies.

Similarly as for the $^7F_0$ state the $^5D_0$ is split into three hyperfine states. One of them is used to achieve the interaction between ions used in CNOT gates. For this purpose the higher energy state is used as an excited state because the ion will change its dipole moment between being in the lower L=3 state and the excited L=2 state. The change in dipole moment gives a change in the dipole-dipole interaction between the ions which then can be used for implementing gate operations.

7

2.7 Dipole-dipole interaction

For a rare earth ion situated in a Yttrium orthosilicate crystal the lattice around will be distorted due to different ion size than the normal Yttrium ion resulting in different permanent electric dipole moment. This change in the crystal will of course affect other ions situated nearby. In this thesis the considered interaction has been between the static electric dipole moments. As stated above the dipole moment for the rare earth ions will change between the ground state and the excited state. This means that exciting one ion induces a change in the crystal which result in a change in energy between the ground state and the excited state for other ions positioned nearby. This change or shift can be expressed using Jackson's equation for dipole-dipole interaction [5]. Since the ions are situated in a crystal a prefactor is used modifying the standard equation with the local field correction using the relative permittivity at zero frequency, also called dielectric constant, for the host material. If an ion has different dipole moment in the ground and the excited state with the difference $\Delta\mu = \mu_g - \mu_e$ then the shift in transition energy between those states for another nearby ion can be written as

$$\Delta E = \frac{(\epsilon(0)+2)^2}{9\epsilon(0)} \frac{|\Delta\mu_1||\Delta\mu_2|}{4\pi\epsilon_0|\mathbf{r}|^3} (\delta\hat{\mu}_1 \cdot \delta\hat{\mu}_2 - 3(\delta\hat{\mu}_1 \cdot \hat{\mathbf{r}})(\hat{\mathbf{r}} \cdot \delta\hat{\mu}_2)) \qquad (4)$$

where the subscript is the first or second ion. $\mathbf{r}$ is the spacial vector pointing from the second ion to the first and ϵ_0 is the permittivity in vacuum. The variables with a hat are unit vectors, so $\delta\hat{\mu}_1$ is the direction of the difference in dipole moment between the ground state and excited state for the first ion. For this type of crystal $\epsilon(0) = 7$ is a normal static relative permittivity [11]. The last factor that just depend on the different unit vectors can be called the geometric factor and this can vary between 1 and -2.

3 Crystal

When choosing a host crystal for rare earth ions a few properties are searched for. Firstly the crystal need to have good optical properties allowing the light pulses to reach the ions and not absorb any of the emitted light. Secondly having a low maximum phonon mode minimizes the possibility for relaxation in the rare earth ions due to phonons in the chrystal. Thirdly a low nuclear magnetic moment from the host atoms ensure that dephasing due to core-electron interaction is minimized. One material that fulfills these properties is Yttrium orthosilicate.

3.1 Y_2SiO_5

The Yttrium orthosilicate crystal is widely used for its optical properties as host crystal. Since both Si and O have no magnetic moment and yttrium only a small of $-0.13\mu_N$ [8] the decoherence due to spin flips which creates a fluctuating field is minimized [7].

   The material crystallizes in a monoclinic cell with space group C 1 2/c 1 (C_{2h}^6). This space group results in the basic molecule appearing eight times in the unit cell due to folding and equivalent positions. In Table 1 is the unit cell parameters and in Table 2 is the position of the basic atoms [10], recalculated from the space group I 1 2/a 1. The two unit cells share the b axis so the different vectors drawn in figure 4 are all in the same plane orthogonal to the b axis. There are two crystallographic different sites that the yttrium ion occupy, Y1 and Y2. When doping with rare earth ions they replace the yttrium ions primarily in site 1 and since the two sites have a difference in resonance frequency of some nm the model is just using site 1 [9]. In table 3 is the Cartesian coordinates to the sites of Y1 which are all crystallographic equal in the unit cell. Using this data the unit cell can be constructed as in figure 3.

parameter	value
a	14.4137Å
b	6.7190Å
c	10.4000Å
α	90°
β	122.235°
γ	90°

Table 1: Unit cell parameters for Y_2SiO_5 [10]

3.2 Implanted ions

Since the qubits are rare earth ions they are doped into the material and replace Y^{3+}. Many of the different rare earth ions could be used but some properties differs between them. Primarily is the number of electrons in the 4f shell different. This affects other properties such as the coherence time. If the number of 4f electrons is odd the magnetic interaction will be strong due to unquenched electronic spin [11]. That is why ions with an even number of 4f electron ions, such as Pr^{3+} and Eu^{3+}, have so long coherence times for their 4f states.Those

Atom	x	y	z
Y1	0.037	0.257	0.466
O1	0.089	0.002	0.143
O2	0.118	0.287	0.318
Si	0.181	0.093	0.308
O3	0.297	0.429	0.060
O4	0.298	0.157	0.33
Y2	0.359	0.122	0.165
O5	0.485	0.102	0.103

Table 2: The basic position of atoms in the unit cell [10]

Axis orientation [Å]		
	x	y	z
a:	-14.4137	0	0
b:	0	6.719	0
c:	5.54729	0	8.79702

Y1 sites in the crystal [Å]		
x	y	z
2.051730	1.726783	4.099411
-5.155119	5.086283	4.099412
-13.691785	1.726785	0.299100
-6.484934	5.086284	0.299099
-10.918139	4.992218	4.697611
-3.711290	1.632717	4.697610
4.825376	4.992216	8.497922
-2.381475	1.632717	8.497922

Table 3: Cartesian coordinates of the eight places for Y1 in the unit cell in Å.
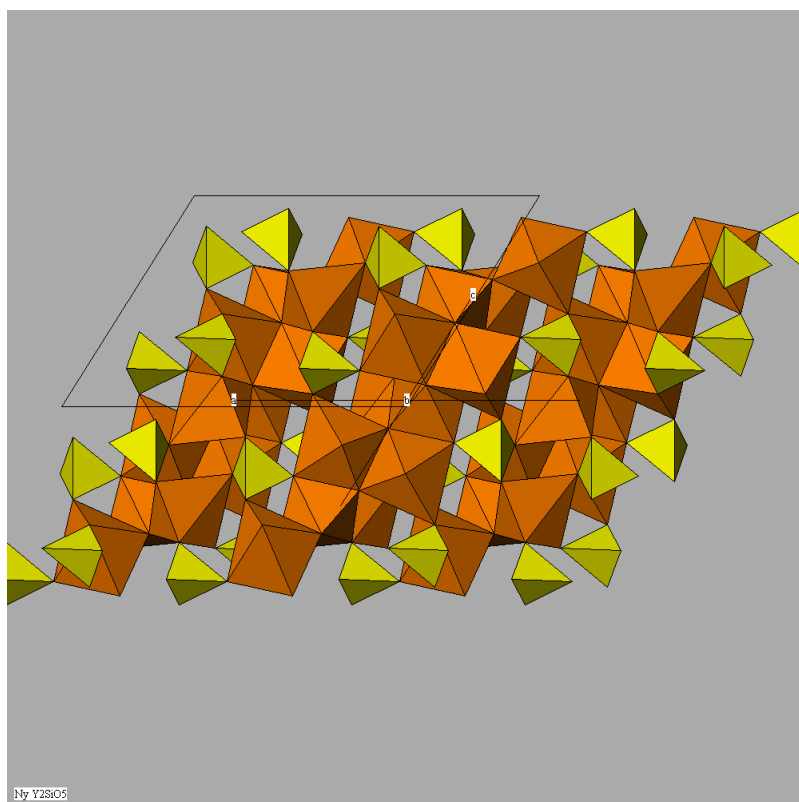
Figure 3: The Y_2SiO_5 crystal along the b-axis with Si atom in the yellow polygons and Y in the orange, from a crystal viewer program
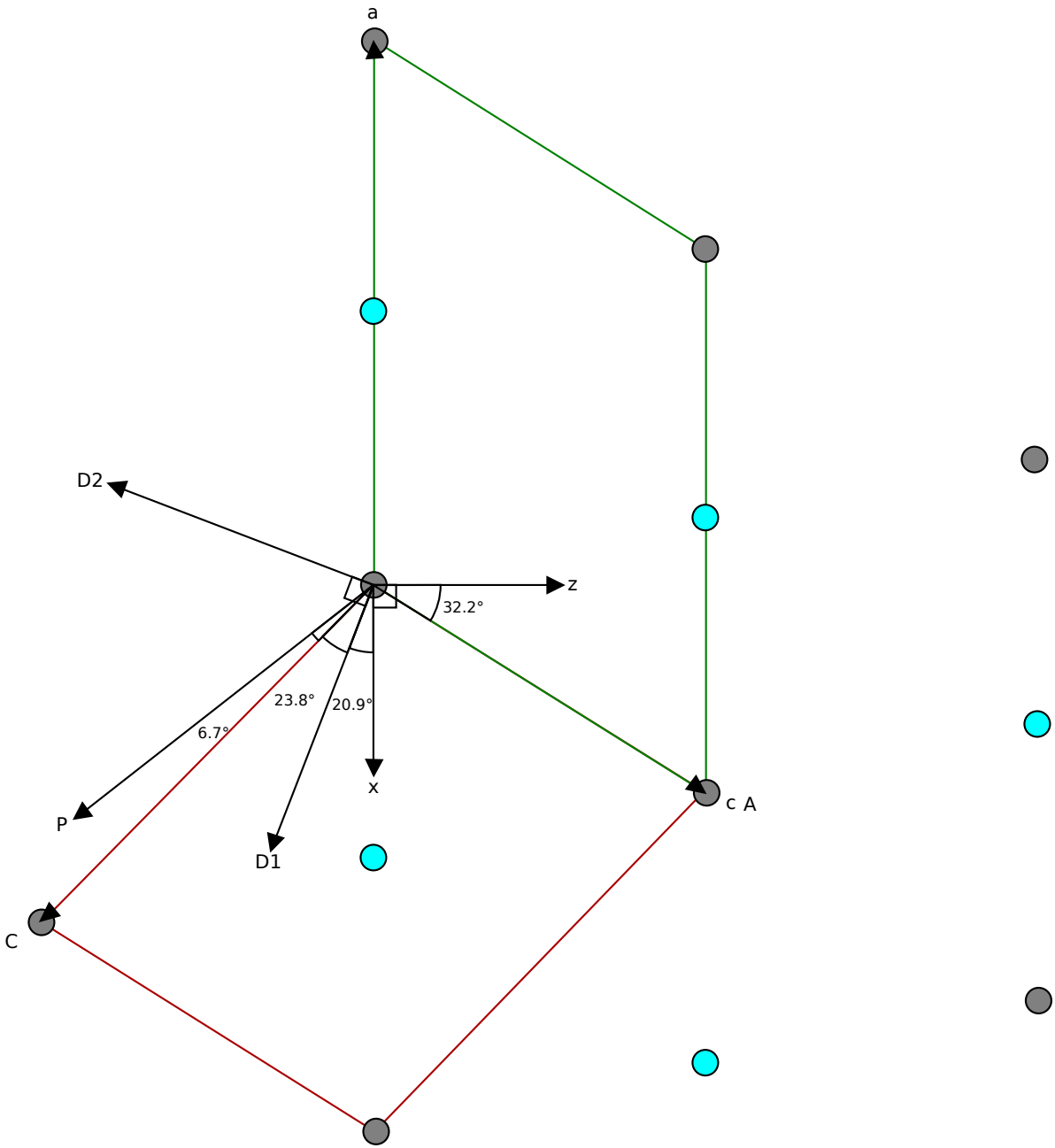
Figure 4: Showing the relations between different vectors in the same plane for the yttium crystal. The grey dots are equivalent crystal points in the plane and the light blue are similar points half a unit cell distance out perpendicular to the plane, parallel with the b axis. The green box is the unitcell for C 1 2/c 1 space group with axis a and c. The red box is the unitcell for I 1 2/a 1 unitcell with the axis A and C. The two principal axis for the crystal, D1 and D2, are also included as are the P vector which together with the b axis spans the plane at which the dipole moment direction lives for Pr. Lastly is the cartesian axis noted with the y axis being parallel with the b axis.

two are the ones used in this thesis. The energy levels for the ions are then affected by the crystal field and split due to the Stark shift. This interaction with the crystal field mixes the state a bit which makes some transitions that normally are forbidden to be weakly allowed [11]. As a consequence the normal term symbol (such as $^3H_4$) is not entirely correct.

3.3 Praseodymium

In Praseodymium the ground level in the 4f shell is $^3H_4$ and the transition studied is between that state and $^1D_2$ as can bee seen in figure 5. Each of the states are split into three levels due to second order hyperfine splitting and electronic quadrupole interaction which is interaction between the core and the electrons. This hyperfine splitting is very small being just a couple of MHz for Pr^{3+}. The energy between the states is 495THz which is visible light in the red region.
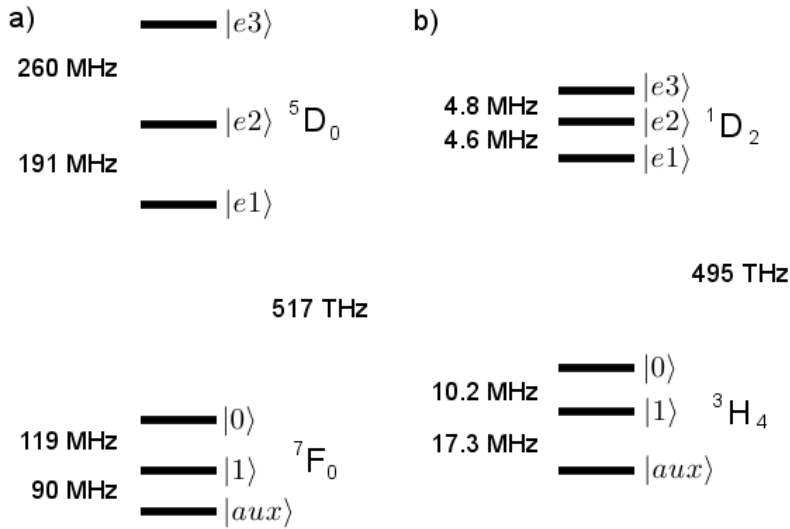
Figure 5: The different levels of a) Eu^{3+} and b) Pr^{3+} with the hyperfine splitting that is used in the thesis

3.4 Europium

The transition studied in Europium is $^7F_0 \leftrightarrow {}^5D_0$ and can be seen in figure 5. A transition with J=0 to J=0 is normally not permitted, but since these are mixed states this transition is weakly allowed giving a long coherence time. Due to similar hyperfine splitting mechanism as for praseodymium the states are also split into three levels each. This level splitting is much larger for Europium, around 100MHz between the levels.

3.5 Read-out ion

When trying to read out the result, that is if an ion is in $|0\rangle$ or in $|1\rangle$, the data should not be destroyed in the sense that it becomes something that it was not.

	Eu^{3+} site I	Pr^{3+} site I	Ce^{3+} site I
$\delta\mu[D]$	$2.3 * 10^{-2}$	$7.3 * 10^{-2}$	0.5

Table 4: The difference in static dipole moment between the ground state and the excited state used with $1D = 3.33 * 10^{-30} Cm$ [4]

To avoid this a special ion is used to read out the data. Since a specific data from one qubit ion is wanted the same goes for the read-out ion where single ion information is wanted. To increase the signal from that single read-out ion the ion is cycled many times between two levels. To be able to use this method the ion need to decay rapidly down to the ground state when excited. The emitted photon from the relaxation is also needed to have another frequency than the pulse frequency sent onto this ion otherwise the emitted photon will be very hard to detect. This is possible if the ground state have some states with a bit higher energy, for example different phonon lines. When relaxing the electron might then relax to a higher phonon line than the ground state first, and thus emit a photon with higher wavelength that can be detected. Using the dipole-dipole interaction a neighboring qubit ion might change the energy for the excited state in the read-out ion so it comes outside the frequency range of the laser pulse driving the read-out cycle resulting in no photons emitted from the read-out ion. Thus a simple way to read out the data from one qubit close enough to a read-out ion is to excite $|0\rangle$ up to $|e2\rangle$ and then apply a pulse that cycles the read-out ion and detecting if any photon with a higher wavelength is emitted.

One such ion that can be cycled is Cerium that have one 4f electron and where the transition between $^2F_{5/2}$ and $^2D_{\frac{3}{2}}$ is used. The second state is in 5d shell, which results in much shorter coherence times since it is outside 5s and 5p, which enables the cycling of the state in the ion and studying the emission. For this to work the emitted light of a single ion needs to be detected and such precision has recently been reached [6].

3.6 Dipole moments

As can be seen in equation 4 the shift in energy depends on the difference in the static electric dipole moment between the ground and excited state for the two ions, the distance between them and the direction of the dipole moments. The distance is given by the position in the crystal and the difference in the static dipole moment between the ground and excited state is given in table 4. About the direction of the change in static dipole moment is known that for Pr ions the angle between them is 24.8 degree in a plane spanned by the b axis and the vector P from figure 4 [3]. Since the basic molecule is folded and mirrored the direction of one is set and the rest follows setting up the dipoles as seen in figure 6.

3.7 Homogeneous and inhomogeneous broadening

The properties of the homogeneous broadening and the inhomogeneous is precisely why rare earth ions in a crystal works as an idea for quantum computing. Since the states that are discussed have so long coherence times the line widths,
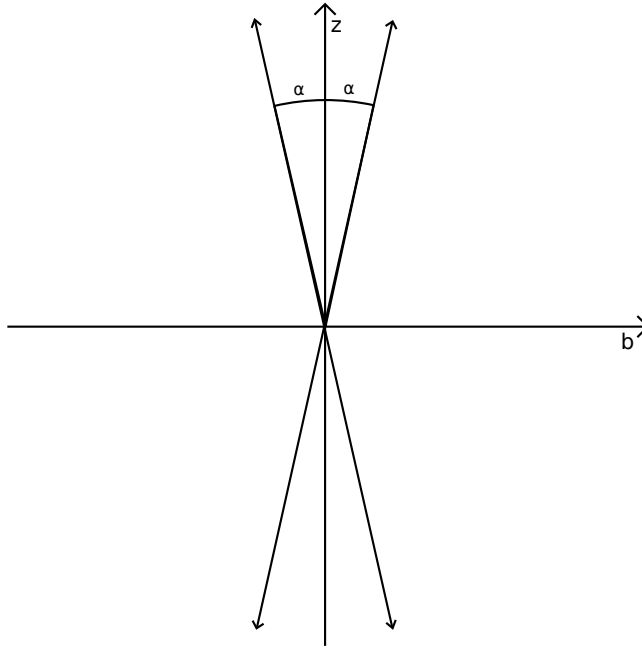
Figure 6: The plane and direction of the change in static dipole moment between ground and excited state.

the homogeneous broadenings, are very small being around kHz or smaller[17]. This since the homogeneous broadening, Γ_h, depend on the coherence time, T_{coh}, by

$$\Gamma_h = \frac{1}{2\pi \mathrm{T}_{coh}} \tag{5}$$

The inhomogeneous broadening however is much larger and depends mainly on the host material for the ions. It comes naturally that the surrounding affects the ion and in a crystal this can be pictured with the crystal field which is the static electric field produced by a surrounding charge distribution. If an impurity, something not normally in the crystal, is in the neighborhood this field will change and so will the levels in the ion and thus the resonance frequency will change. In a macroscopic doped crystal the surrounding for each ion that is doped into the crystal will be different resulting in different shifts of the resonance frequency. Summing up all the new resonance frequencies gives the inhomogeneous broadening for the rare earth ions and is on the order of GHz. Due to the shift in resonance frequency being dependent of different surroundings of the ions it is no surprise that different doping concentrations will affect the broadening. For Eu doped in Y_2SiO_5 the inhomogeneous broadening can be modeled by a normal distribution with

$$\mathcal{N}\left(0, \left(\frac{\Gamma_{ih}}{2\sqrt{2ln(2)}}\right)^2\right) \tag{6}$$

where the inhomogeneous broadening $\Gamma_{ih} = \Gamma_{ih0} + \Gamma_{ihK}\mathrm{C}_{Doping}$ with C_{Doping} being the atm doping concentration between 0 and 1. As can be seen this

15

model has a term which is doping concentration independent. From [15] the values $\Gamma_{ih0} = 1.8\text{GHz}$ and $\Gamma_{ihK} = 1800\text{GHz}$ is used.

That the inhomogeneous broadening is so much larger than the homogeneous means that ions can individually be targeted. Each ion has a small channel in the frequency range where transitions will happen and this channel is depending on the surrounding and situated somewhere within the large broadening. If the resonance frequency for each ion is randomized, since it is a thesis in itself to find how to calculate a reasonable non-randomized broadening, the probability that two neighboring ions will overlap in frequency is very small. Combining with the fact that the dipole-dipole interaction is very dependent of the distance the result is a high probability that a single ion can be targeted and used for interaction with neighboring ions without loss in fidelity due to interference from other ions.

4 Evolution in time

For every answer there is a correct question. Thus to understand a system such as rare earth ions in a crystal, simply analyzing in steady state can only give that much answers. A natural follow-up is to move into the time regime and analyze the individual trees instead of the forest. To this end the time dependent Schrödinger equation was used.

$$H(t)\,|\psi(t)\rangle = i\hbar\frac{d}{dt}\,|\psi(t)\rangle \tag{7}$$

Solving this equation exact analytically is close to impossible for most cases resulting in the use of simplifications or numerical solutions. To this end the time from $t = 0$ to $t = \tau$ where τ is the time the operation ends is cut to pieces. In each time step, Δt, the Hamiltonian is assumed to be constant. Knowing the start value for the wave function the wave function at time Δt can be calculated using $n = 0$ in

$$|\psi([n+1]\Delta t)\rangle = e^{\frac{-i\Delta t}{\hbar}H([n+1/2]\Delta t)}\,|\psi(n\Delta t)\rangle \tag{8}$$

This can be evolved to

$$|\psi([n+1]\Delta t)\rangle = e^{\frac{-i\Delta t}{\hbar}\lambda([n+1/2]\Delta t)}\,|\nu([n+1/2]\Delta t)\rangle\,\langle\nu([n+1/2]\Delta t)|\psi(n\Delta t)\rangle \tag{9}$$

where λ and ν are the eigenvalues and the eigenvectors to the hamiltonian. By iterating this step and letting the known start wave function evolve the time dependent Schrödinger equation can be solved numerically. As Δt is made infinitely small the result approach the exact solution to the SE. What remains is to find a Hamiltonian for the system.

4.1 Hamiltonian

In a three level system the Hamiltonian is a three by three matrix and can be divided into two matrices H_0 containing the energies on the diagonal and H_1 containing the interaction terms on the off diagonals [14]. The energies are fairly simple being expressed in $\hbar\omega$ with ω being the rotation frequency and in unit [rad/s]. Since the system in our case is driven and exposed to light which has a frequency of hundreds of terahertz and the splitting between $|0\rangle$ and $|1\rangle$ is at MHz range the interaction between them is set to zero. For the other interaction terms the electric dipole interaction gives that they are $-\vec{d}\cdot\vec{E}$. The electric field where ω_L is the frequency of the light pulse is expressed as

$$\vec{E} = \frac{\vec{E_0^*}e^{-i\omega_L t} + \vec{E_0}e^{i\omega_L t}}{2} \tag{10}$$

and the dipole moment operator as

$$\vec{d} = -(\vec{d_{ge}}\,|0\rangle\,\langle e| + \vec{d_{ge}^*}\,|e\rangle\,\langle 0| + \vec{d_{ge}}\,|1\rangle\,\langle e| + \vec{d_{ge}^*}\,|e\rangle\,\langle 1|) \tag{11}$$

where it is assumed that the two states $|0\rangle$ and $|1\rangle$ have the same dipole moment and can be seen as a common ground state $|g\rangle$ for dipole matters. Then $\vec{d_{ge}}$ can be defined as $\vec{d_{ge}} = \langle g|\,\vec{d}\,|e\rangle$. Multiplying them and defining

$$\Omega = \frac{\vec{d_{ge}}\vec{E_0}}{\hbar} \tag{12}$$

$$\tilde{\Omega} = \frac{\vec{d_{ge}}\vec{E_0^*}}{\hbar} \tag{13}$$

result in

$$H_1 = -\frac{\hbar}{2}((\Omega e^{i\omega_L t} + \tilde{\Omega}e^{-i\omega_L t})\left|1\right\rangle\left\langle e\right| + (\Omega^* e^{-i\omega_L t} + \tilde{\Omega}^* e^{i\omega_L t})\left|e\right\rangle\left\langle 1\right|$$
$$+ (\Omega e^{i\omega_L t} + \tilde{\Omega}e^{-i\omega_L t})\left|2\right\rangle\left\langle e\right| + (\Omega^* e^{-i\omega_L t} + \tilde{\Omega}^* e^{i\omega_L t})\left|e\right\rangle\left\langle 2\right|) \tag{14}$$

This Hamiltonian contain both fast rotating terms and slow rotating terms wich can be clearly seen by taking it into the Dirac picture. After doing rotating wave approximation [1] and removing the fast rotating terms where the frequency of the light and the frequency of the excited states add since they will fast average out to zero, the hamiltonian still in Dirac picture is

$$H_{1DP} = -\frac{\hbar}{2}(\Omega e^{i(\omega_L - \omega_e)t}\left|1\right\rangle\left\langle e\right| + \Omega^* e^{-i(\omega_L - \omega_e)t}\left|e\right\rangle\left\langle 1\right|$$
$$+ \Omega e^{i(\omega_L + \omega_2 - \omega_e)t}\left|2\right\rangle\left\langle e\right| + \Omega^* e^{-i(\omega_L + \omega_2 - \omega_e)t}\left|e\right\rangle\left\langle 2\right|) \tag{15}$$

The full hamiltonian in Schrödinger picture is then

$$H = \begin{bmatrix} \hbar\omega_0 & 0 & -\frac{\hbar\Omega(t)}{2}e^{i(\omega_L t + \phi)} \\ 0 & \hbar\omega_1 & -\frac{\hbar\Omega(t)}{2}e^{i(\omega_L t + \phi)} \\ -\frac{\hbar\Omega^*(t)}{2}e^{-i(\omega_L t - \phi)} & -\frac{\hbar\Omega^*(t)}{2}e^{-i(\omega_L t - \phi)} & \hbar\omega_e \end{bmatrix} \tag{16}$$

4.2 Rotating frame

When the above Hamiltonian is implemented and the evolution in time of the wave functions are tried it is easy to understand that the time steps need to be very small since it must resolve the frequency of the light which is at terahertz. Doing that take much time from better things so to avoid the problem a rotating frame is introduced. It is best understood by letting a unitary operator work on the Hamiltonian that will create a rotating frame that rotates the third energylevel.

$$U = \begin{bmatrix} 1 & 0 & 0 \\ 0 & 1 & 0 \\ 0 & 0 & e^{-i\omega_{RF}t} \end{bmatrix} \tag{17}$$

Applying this transformation on the time dependent Schrödinger equation

$$U^\dagger H\left|\psi\right\rangle = i\hbar U^\dagger \frac{d}{dt}\left|\psi\right\rangle \tag{18}$$

$$H'\left|\psi_{RF}\right\rangle = i\hbar U^\dagger(\frac{dU}{dt}\left|\psi_{RF}\right\rangle + U\frac{d}{dt}\left|\psi_{RF}\right\rangle) \tag{19}$$

$$\left(H' - i\hbar\begin{bmatrix} 0 & 0 & 0 \\ 0 & 0 & 0 \\ 0 & 0 & -i\omega_{RF} \end{bmatrix}\right)\left|\psi_{RF}\right\rangle = i\hbar\frac{d}{dt}\left|\psi_{RF}\right\rangle \tag{20}$$

where $H' = U^\dagger H U$ and $\left|\psi_{RF}\right\rangle = U^\dagger\left|\psi\right\rangle$ which gives an effective Hamiltonian

$$H_{RF} = \begin{bmatrix} \hbar\omega_0 & 0 & -\frac{\Omega(t)}{2}e^{i(\omega_L - \omega_{RF})t + i\phi} \\ 0 & \hbar\omega_1 & -\frac{\Omega(t)}{2}e^{i(\omega_L - \omega_{RF})t + i\phi} \\ -\frac{\Omega^*(t)}{2}e^{-i(\omega_L + \omega_{RF})t - i\phi} & -\frac{\Omega^*(t)}{2}e^{-i(\omega_L + \omega_{RF})t - i\phi} & \hbar(\omega_e - \omega_{RF}) \end{bmatrix} \tag{21}$$

Increasing the frequency of the rotating frame, ω_{RF}, to about the same frequency as the light reduces the exponent and thus the frequency of the interaction term and so larger timesteps can be taken while keeping it well resolved.

4.3 Many Ions

The Hamiltonian in (21) does just explain a system of one ion. When expanding the system to include more ions the Hamiltonian must of course expand as well. Just thinking about the eigenstates for two ions instead of one ion the eigenstate for the ground level changes from $|0\rangle$ to $|00\rangle$ since the state of the two of them need to be explained. This gives that the Hamiltonian for two ions will be a 9×9 matrix and more generally the n ion Hamiltonian will be a $n^3 \times n^3$ matrix. Constructing this Hamiltonian for two ions is done by

$$H_{RF}^2 = H_{RF}^1 \otimes \mathbb{1} + \mathbb{1} \otimes H_{RF}(2) + H_{DDinteraction} \tag{22}$$

where $\otimes$ is a tensorproduct. The superscript of H_{RF} note the complete hamiltonian for that number of ions and the paranthesis note the basic hamiltonian with the energylevels of that ion. $H_{DDinteraction}$ is zeros except for the matrix element where two of the ions are in the excited state, that is $\langle ee|ee \rangle = \hbar \Delta E$ where ΔE is the dipole-dipole interaction term between the two ions in Rad/s. Following similar way an algorithm for making a Hamiltonian for a general number of ions can be made.

4.4 Pulses

When applying a pulse to the system the interaction terms in the Hamiltonian, that is the off diagonal terms change depending on the frequency of the incoming light pulse and the Rabi component which describes how the pulse behaves in time. The pulse is described with

$$-\frac{\hbar \Omega(t)}{2} e^{i(\omega_L t + \phi)} \tag{23}$$

where $\Omega(t)$ is the Rabi frequency, ω_L is the frequency of the light and ϕ is the phase.

What is done before is to describe the model but the toolbox that will be used is the pulses. Since the superposition between $|0\rangle$ and $|1\rangle$ can be described by a vector on the Bloch sphere the effect of the pulses are also well described using Bloch vectors.

There are many different kinds of pulses, the easiest being a square pulse, where a laser with a fix frequency and phase is on for a time period and otherwise off. This pulse, depending on the phase, rotates the Bloch vector around x- or y-axis with an angle corresponding to the area under the Rabi frequency which depends on the intensity of the beam. A π rotation can be done by setting $\Omega(t) = 10^6$Rad/s and applying the pulse for a duration of $\pi * 10^{-6}$s where in this case the area correspond to the product between the time and Rabi frequency.

Since in nuclear magnetic resonance (NMR) a lot of different pulses are used and have been used for a long time, many pulses have been developed by them. One such pulse is the complex hyperbolic secant pulse, so called sechyp, which

is very good on one thing, to swap the probabilities between two states. With a normal square pulse a π pulse will swap the probabilities as well, but as soon as the resonance frequency is a bit off the laser frequency the rotation will no longer be around the x- or y-axis and so give a loss in fidelity. The sechyp however start the pulse by rotating the Bloch vector in the x-y plane in one direction then do the transfer with a Rabi frequency varying but with the area equal to π and end rotating the other way in the x-y plane, see figure 7. This way, as long as the detuning, that is the difference in frequency between the resonance frequency and the frequency of the light pulse, is less than the frequency by which the bloch vector is rotated in the start and end of the pulse the pulse will do a mostly complete transfer (figure 8). The phase of the starting Bloch vector does not matter and the end phase is hard to know since it will be different for different detuning. For the sechyp pulse the Rabi frequency is written as

$$\Omega(t) = \Omega_0(sech(\beta(t - t_0)))^{1+i\mu} \tag{24}$$

Typical values used in experiments for Pr are $\Omega_0 = 0.55 * 2\pi \text{Mrad/s}, \beta = 1.47\text{MHz}, \mu = 1.93$ [13].
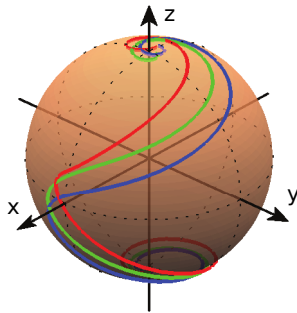
Figure 7: The rotation of the bloch vector for ions with different detuning driven by a sechyp pulse from [12].

Sechyp pulses can also be sent in with two different light frequencies at the same time, so called two color pulses. This is only usable for three levels, where the transfer between two states, $|0\rangle$ and $|1\rangle$, are done via a third state, $|e\rangle$. Letting the pulses have the same Rabi frequency they can be written as $\Omega(t)e^{-i\gamma_0}$ and $\Omega(t)e^{-i\gamma_1}$ where γ is the phase of the light. To better understand how the two-color pulses works another basis between the two data states can be chosen as

$$|\hat{0}\rangle = \frac{1}{\sqrt{2}}(|0\rangle - e^{i\phi} |1\rangle) \tag{25}$$

$$|\hat{1}\rangle = \frac{1}{\sqrt{2}}(|0\rangle + e^{i\phi} |1\rangle) \tag{26}$$

If the phase between the pulses is ϕ then only $|\hat{1}\rangle$ couples to the excited state, called the bright state, while $|\hat{0}\rangle$ can be seen as a dark state [13]. For a phase difference of $\phi + \pi$ the opposite is true. Using the first two two-color pulses from table 5 the probability to be in $|\hat{1}\rangle$ is transfered to the excited state and then
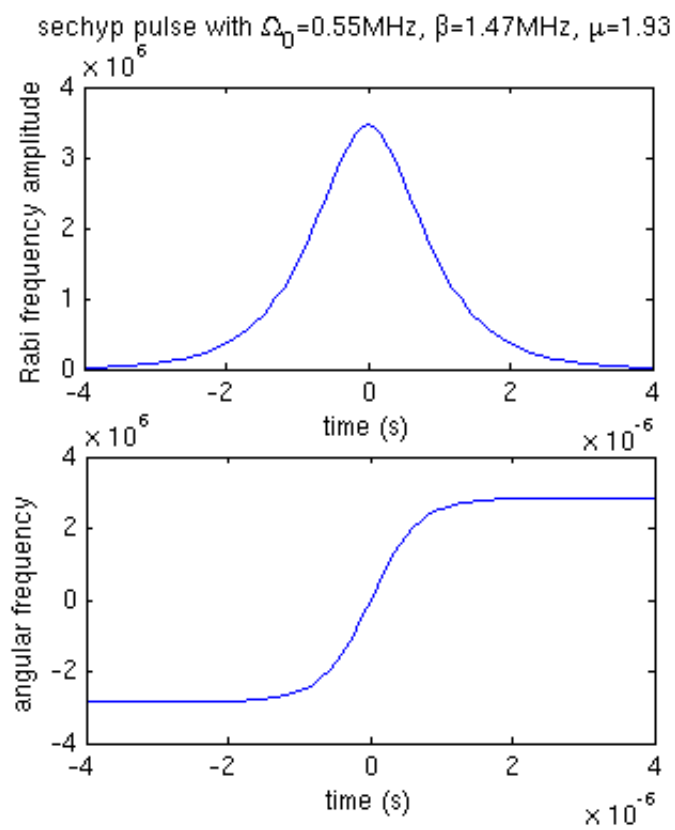
Figure 8: The amplitude and frequency of a sechyp pulse

returned with an arbitrary angle θ. This can be written as $|\hat{1}\rangle \rightarrow |\hat{1}\rangle e^{i\theta}$. In the system this changes the Bloch vector with the angle θ in the plane orthogonal to $|\hat{1}\rangle$ from how it was before. Changing the value of ϕ the state $|\hat{1}\rangle$ changes and thus the plane in which the rotation is done. Normally this value is either $\pi/2$ for rotation around the y-axis or π for rotation around x-axis.

This is true for ions with the resonance frequency at the light frequency. For ions that are detuned from this frequency another phase angle will appear that depends on the detuning. To remove this extra phase that is added to $|\hat{1}\rangle$, the same phase is added to $|\hat{0}\rangle$ making it a global phase of the states that does not change the relative phase between the states and thus does not affect the Bloch vector. This phase is added by applying similar pulses as before but without any angle change targeting $|\hat{0}\rangle$.

Pulse #	φ_0	φ_1	$\varphi_1 - \varphi_0$	Description
1	0	ϕ	ϕ	$|\hat{1}\rangle \rightarrow |e2\rangle$
2	$\pi + \theta$	$\pi + \phi + \theta$	ϕ	$|e2\rangle \rightarrow |\hat{1}\rangle$ with angle θ
3	0	$\pi + \phi$	$\pi + \phi$	$|\hat{0}\rangle \rightarrow |e2\rangle$ to compensate
4	π	$2\pi + \phi$	$\pi + \phi$	$|e2\rangle \rightarrow |\hat{0}\rangle$ to compensate

Table 5: Angles for the four two color pulses. If $\phi = \pi$ the rotation is around the x-axis and if $\phi = \frac{\pi}{2}$ the rotation is around the y-axis, [13]

4.5 Raman transitions

Since the two-color pulses have two frequencies at the same time the possibility for two photon processes appear. Such a process is the Raman transition where an electron is excited up to a virtual state and deexcited to the other ground state. This process can be described with adiabatic Raman transition which for the space spanned by the states $|0\rangle$ and $|1\rangle$ can be expressed as transformation operator

$$U = e^{-\frac{i}{2}\Lambda_2 \vec{\sigma} \cdot \vec{n}} \tag{27}$$

where $\vec{\sigma}$ is the vector of Pauli matrices and a rotation Λ_2 around an axis described by unit vector $\vec{n}$. Those are defined as

$$\Lambda_2 = \int_{t_i}^{t_f} -2\sqrt{\Omega^2(u) + \left(\frac{\Delta}{2}\right)^2} \sin^2\left(\frac{1}{2}\arctan\left(2\frac{\Omega(u)}{\Delta}\right)\right) du \tag{28}$$

$$n_x = \cos(\alpha)\sin(2\arctan(1)) \tag{29}$$

$$n_y = -\sin(\alpha)\sin(2\arctan(1)) \tag{30}$$

$$n_z = \cos(2\arctan(1)) \tag{31}$$

with α being the phase between the two pulse frequencies [2].

5   Results

Coming this far into the thesis the theories are waiting to be applied onto som results. Starting quite general step by step the results will approach simulating a quantum computer algorithm. The first results come from analysing doped ions in the crystal-model and a possible way to compare results from the model with real world results through the echo experiment. A single ion is then exposed to different pulses and analysed. Expanding the Hamiltonian multiple ions and their interactions are analysed. Last is the possibility to make chains of qubits explored in a simplified way.

5.1   Qubit interaction and frequency shifts

5.1.1   Doping and shift statistics

The key to be able to do any quantum computing is the read-out process. Without the read-out ion nothing that happens will have any impact on the world. Thus the interaction between the Ce ion and the Pr ions is studied. To understand the basic interaction between two ions and to what extent the shift depend on the distance between them a figure such as figure 9 is a step on the way. In the figure the dipole-dipole interaction in equation 4 between a Ce ion and a Pr ion is used with the directions of the dipole moment change being parallel to each other and orthogonal to the vector $\bar{\mathbf{r}}$ resulting in a geometrical factor of 1.
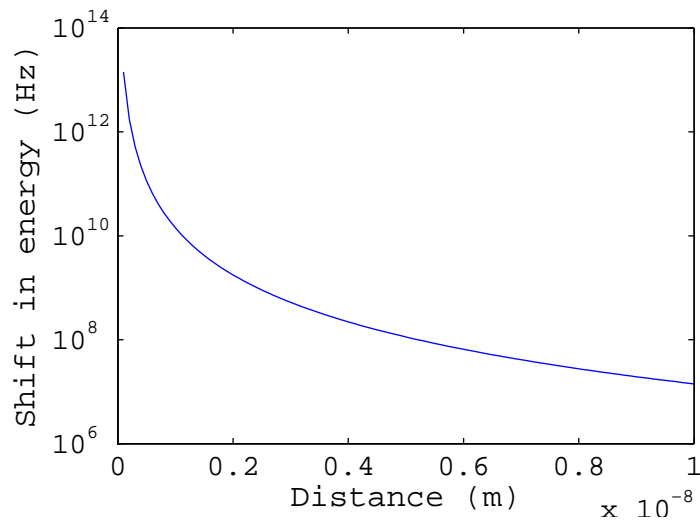
Figure 9: The shift from dipole dipole interaction on a Ce ion from a Pr ion as a function of distance with the dipole moment direction being parallel with each other and with the line between the ions.

As the rare earth ions are situated in a host crystal certain sites are available for the ions. Thus using the model for the yttrium ortho silicate crystal the Y1 site is used and qubit ions are placed randomly corresponding to the doping concentration. The different realizations were made with the ions placed within

23

a sphere with the read-out ion in the middle. From a thousand such realizations for doping concentration 0.1%, 0.2%, 0.5% and 1% the largest shift on the Ce ion from a Pr ion was noted in figure 10 and figure 11. Notable is that for larger shifts just certain lines exist in the shift. This is as expected since just certain sites can be populated and since the interaction highly depends on the distance. Note also that this is the absolute value of the shift.
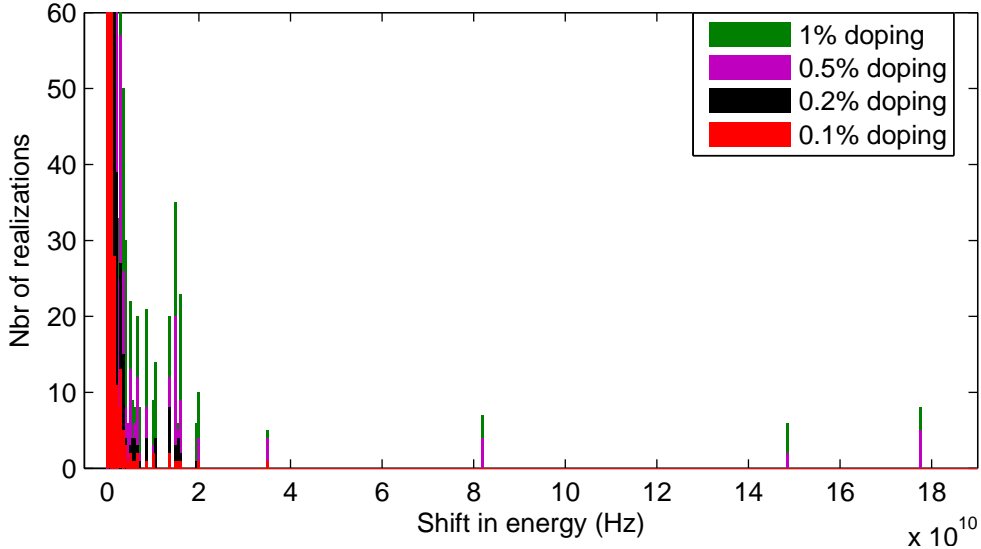
Figure 10: Number of realizations as a function of the shift in energy. From 1000 realizations per doping concentration is the absolute value of the biggest shift on the Ce ion from any Pr ion taken.

The two figures have different scale and figure 11 show the realizations where the read-out ion was nog shifted so much. To know the statistical probability that at least one ion in a realization will be able to shift the read-out ion as much as needed to get some information is very useful when deciding the doping concentration of the crystal. Note that the shift in figure 11 is also in absolute value showing the distribution for the thousand realizations. As the direction of dipole moments is distributed with the mean value zero, half will shift upward and half will shift downward.

It is not only the existance of a qubit that can be read out that is important. If other ions in the crystal are excited by the pulse meant to excite the strongest influencing ion on Ce and the sum of their shifts on Ce is larger than the line width for Ce, that is 3MHz, it is possible that the read out process is corrupted. For this purpose a profile with the probability for a Pr ion with six levels to be excited from a sechyp pulse with the typical parameters in section 4.4 as a function of the detuning, the difference between the resonance frequency of the ion and the frequency of the incoming light, can be seen in figure 12. Centering this profile around the resonance frequency of the strongest interaction ion on the read-out ion, all other ions that have a resonance frequency within this profile will be excited with a certain probability. Summing up the shift on the read-out ion from all the ions that are excited together with the strongest influencing
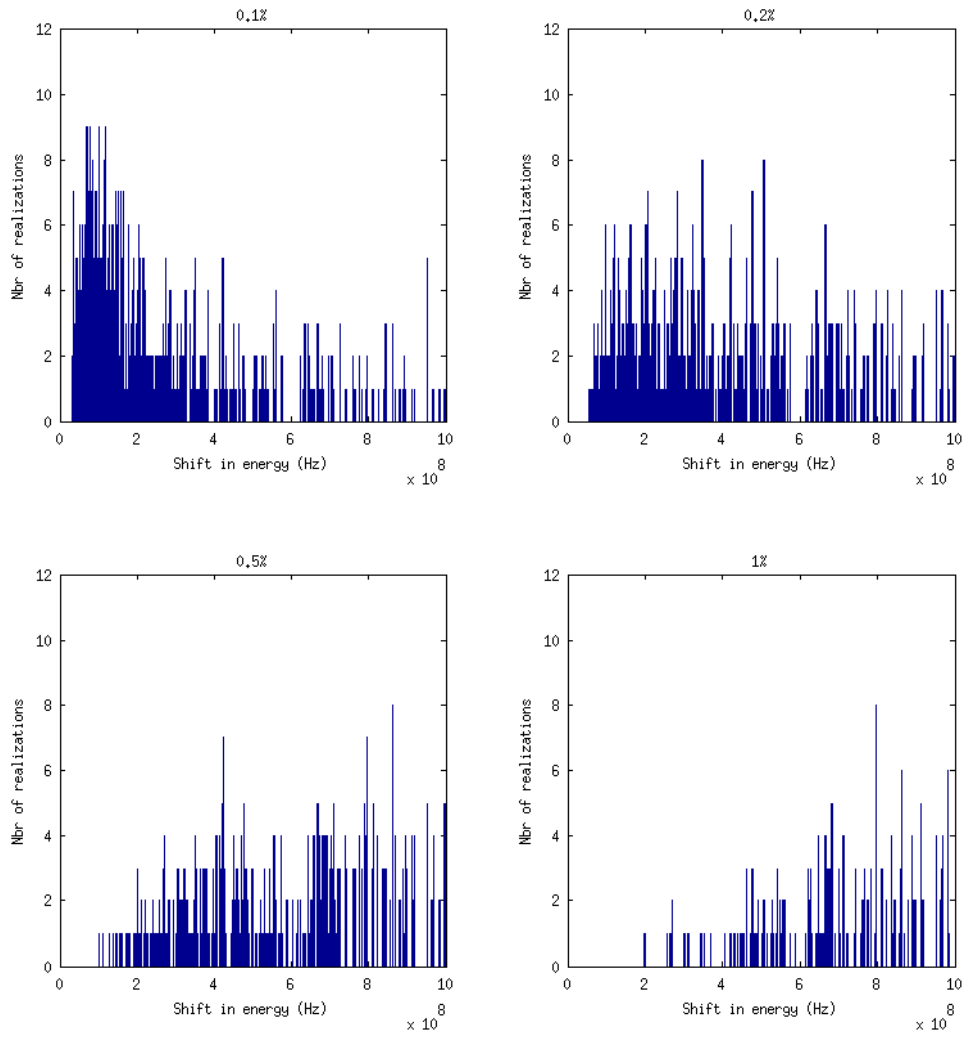
Figure 11: Number of realizations as a function of the shift in energy. This figure shows the same data as figure 10 but focuses on how the probability to get a low interaction changes with changed doping concentration
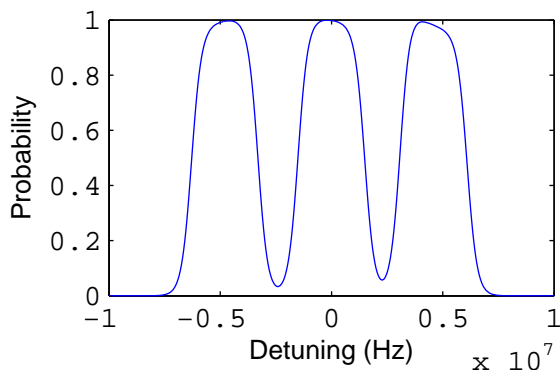
Figure 12: The probability to excite a Pr ion with a sechyp pulse as a function of the detuning

Doping concentration	% shift more than 3MHz	Average (MHz)
0.1%	9.7	1.25
0.2%	14.4	1.69
0.5%	15.2	1.71
1%	17.6	1.86

Table 6: A thousand realizations where the sum of the shifts on the Ce ion from the Pr ions in the crystal within the profile for different doping concentrations was collected

one for a thousand realizations and for 0.1% and 1% doping concentration the histogram in figure 13 was acquired. In table 6 the percentage from a thousand realizations where the sum of the shifts on the read-out ion more than 3MHz and the average shift in energy for four different doping concentrations are noted. Interesting to see is that one magnitude higher doping concentration result in a doubling of realizations where the shift is larger than the Ce linewidth.

Another interesting simulation is how much all the Pr ions (independent of their resonance frequency) outside a range of 10nm shift the resonance frequency of one Pr ion depending on the doping concentration. In figure 9 the magnitude of the shift for 10nm is the same as the detuning needed to be unaffected by the pulse for Pr, which is shown in figure 25. This could result in influence on the target ion from ions far away that disrupts the computation. Ideal would be that the shift from ions further away than 10nm were negligible. To do this a crystal sphere with a diameter of 80nm is setup and a ion in the middle selected. From a thousand realizations the largest negative shift[1] from one ion per realization for the doping concentrations 0.1%, 0.2%, 0.5% and 1% is collected and displayed in figure 14 and the sum of the shifts is displayed in figure 15. The distribution is as expected where the increase in doping concentration also increases the shift. The sum of the shifts show that at a doping concentration of 1% the broadening of the shift in resonance frequency of the target ion reaches roughly 50MHz which compared to the results in section 5.2 is on a magnitude that would disrupt the

---

[1]The largest positive shift give the same result but with opposite sign
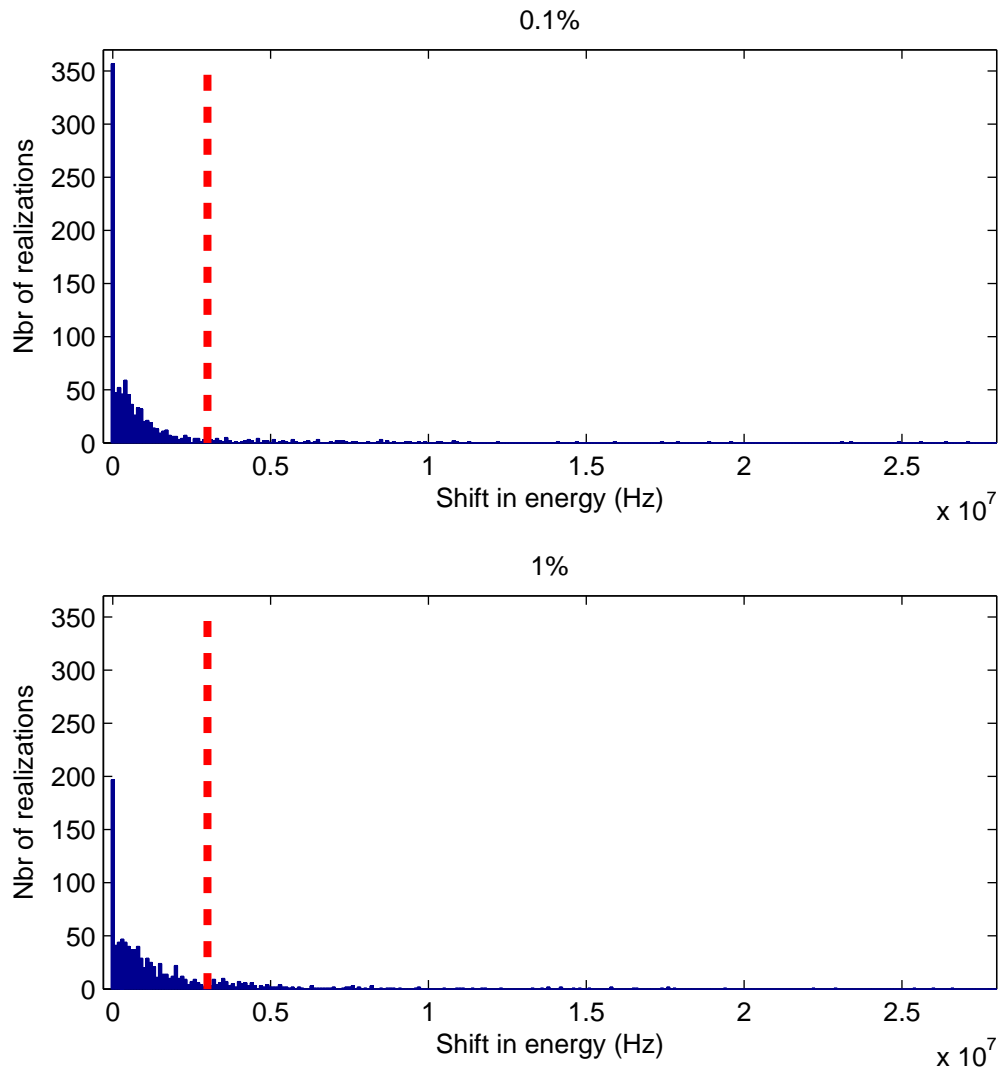
Figure 13: Number of realizations as a function of the shift in energy. For 1000 realizations at doping concentration 0.1% and 1% is the shift on Ce from all excited Pr ions within the sechyp profile taken. The dashed line shows where the 3MHz line is corresponding to the linewidth of Ce.

interaction between the target and close ions used in a computation.
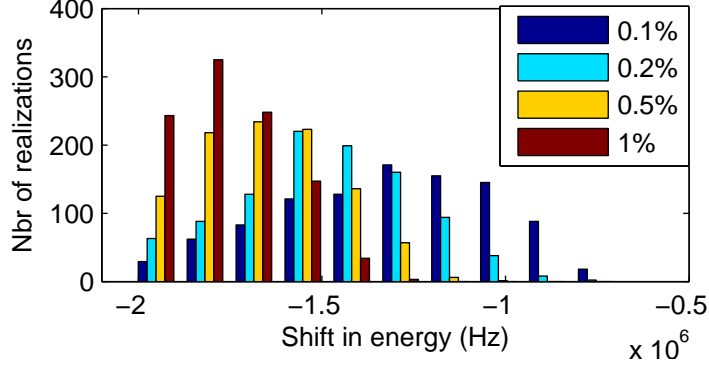
Figure 14: Number of realizations as a function of the shift in energy. The shift from the ion which has the largest negative shift on one Pr ion from Pr ions 10nm away or more for a thousand realizations and different doping concentrations
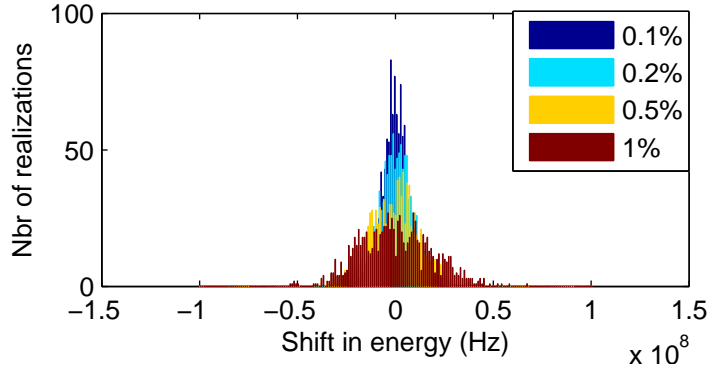
Figure 15: Number of realizations as a function of the shift in energy. The shift on one Pr ion from all Pr ions further away than 10nm for different doping concentrations

5.1.2 Photon echo

The difference in dipole moment between the ground state and the excited state for Ce was calculated from photon echo experiments assuming a lorenzian distribution of the shifts so to test the model and study if the shift follows a lorentzian distribution we model a photon echo experiment with the calculated Ce dipole moment value. The photon echo experiment is done on a crystal with 0.08% Ce^{3+} and 0.05% Pr^{3+}. The Pr is first excited with a $\frac{\pi}{2}$ pulse followed by an excitation pulse to Ce and then a π pulse to Pr. If a Pr ion is shifted in frequency by the excited Ce ions then the time development of the phase will change. After the π pulse to the Pr, Ce is no longer excited which results in the development being different for those Pr ions that were shifted by Ce which results in a weaker echo. Using the model the crystal can be

built up. Assuming that there is no interaction between Ce ions the shift due to dipole-dipole interaction on each Pr ion from all the Ce ions is simulated. This assumption turns out to be reasonable. The Pr ions that are selected in our simulation are within 1GHz of the zero detuning in the inhomogeneous broadening done with a normal distribution with $\sigma = 40$GHz. The Ce ions are within 100MHz of the zero detuning as well but with the inhomogeneous broadening having $\sigma = 4$GHz. These values are reasonable values from the quantum information group at Lund. The resulting shifts are displayed in figure 16 with linear scale on the y axis and figure 17 with logarithmic scale on the y axis.
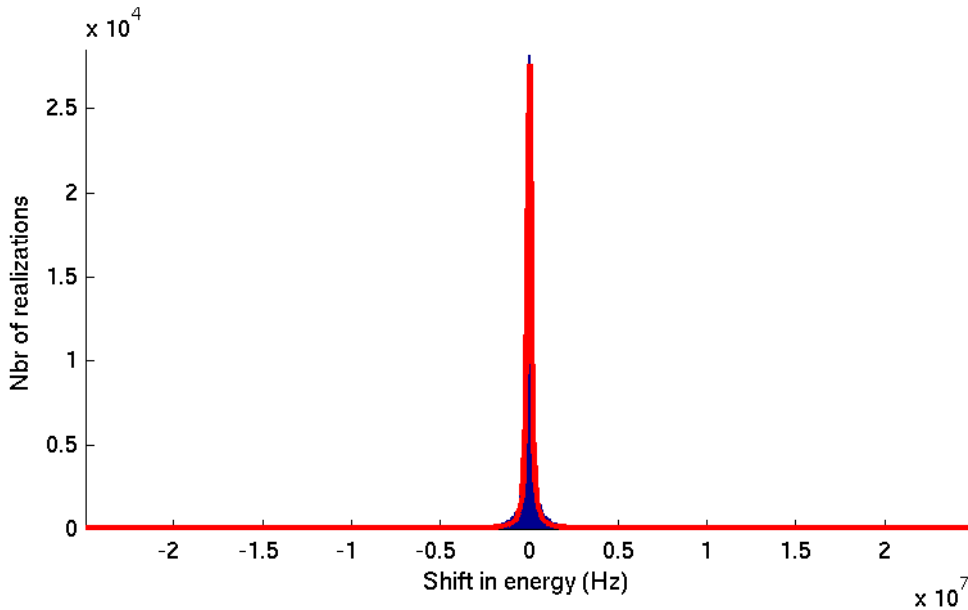
Figure 16: Number of realizations as a function of the shift in energy. A simulation on how the distribution of the shift on Pr ions from all Ce ions will look like

To this distribution a non linear fitting was made with the Lorentzian distribution

$$f(x) = k\frac{1}{\pi}\frac{\left(\frac{\Gamma}{2}\right)^2}{E^2 + \left(\frac{\Gamma}{2}\right)^2} \tag{32}$$

Since the input energy is in Hz Γ will also have the unity Hz. The fitting resulted in $\Gamma = 55$kHz and $k = 9.51 * 10^{10}$. Notable is the shift distribution fits well with the lorentzian for small shifts but falls of slower than the lorentzian distribution.

5.2 Single qubit dynamics

5.2.1 Single-color pulses

To simulate quantum gates an ion is placed alone in the universe and exposed to single-color sechyp pulses with pulse parameters from section 4.4. The ion has all six levels and a NOT operation is done with a pulse between $|0\rangle$ and
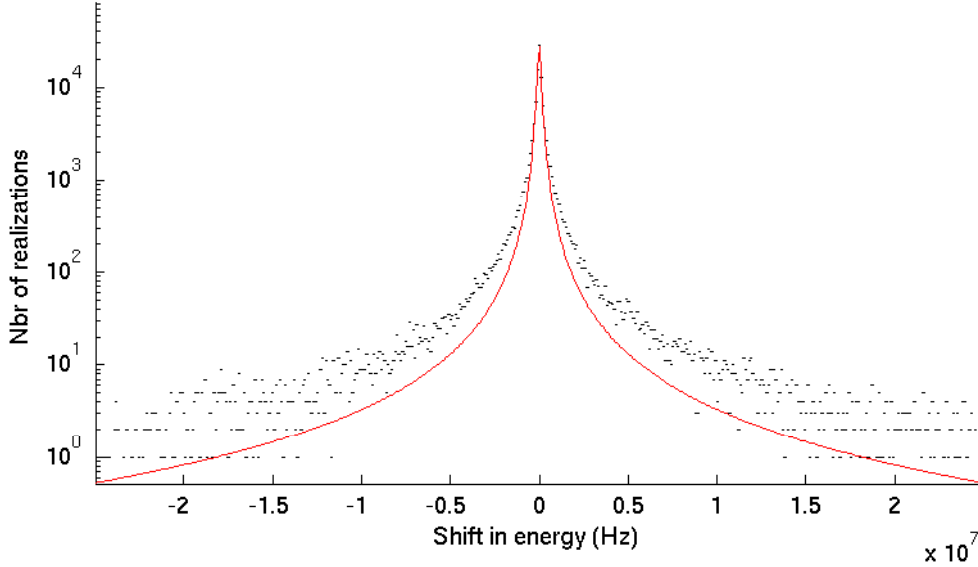
Figure 17: Number of realizations as a function of the shift in energy. A simulation on how the distribution of the shift on Pr ions from all Ce ions will look like with logarithmic scale

$|e2\rangle$ followed by a pulse between $|e2\rangle$ and $|1\rangle$ and last a pulse between $|0\rangle$ and $|e2\rangle$ again. In figure 18 the end result after the operation on a Pr ion is given as a function of the detuning between the light frequency and the resonance frequency of the ion. As shown in the figure is the NOT operation successful for small detunings and leaves ions detuned more than 1MHz unchanged. At the right side the beginning of the next hyperfine level is starting to show.

Changing the pulse parameters to $\Omega_0 = 5 * 2\pi$Rad/s, $\beta = 1.7$MHz and $\mu = 2.69$ and doing the same operation figure 19 is acquired. Now the effect of the nearby hyperfine level is clearly visible. The increase in the frequency range of the pulse broadens the profile resulting in a larger range in frequency where ions are transfered with a high fidelity through the operation.

When instead of Pr an Eu ion with much larger hyperfine splitting is targeted with the same pulse parameters the result is shown in figure 20. It is very similar to figure 19 except that no excitation due to a hyperfine level is seen.

5.2.2   Two-color pulses

Furthermore is the ion exposed to two-color pulses following the scheme and sechyp pulse parameters from section 4.4 with a π rotation around the x axis resulting in a NOT operation. The pulse durations are $8\mu s$ each with the center of the sechyp pulses after half the time. The total NOT operation for an ion in resonance is seen in figure 21. In that figure the last two pulses, the compensation pulses, do not have any effect since zero detuning does not give an extra phase angle. With an ion detuned 1MHz from the light frequency the same operation results in figure 22 where the last two pulses clearly compensate for
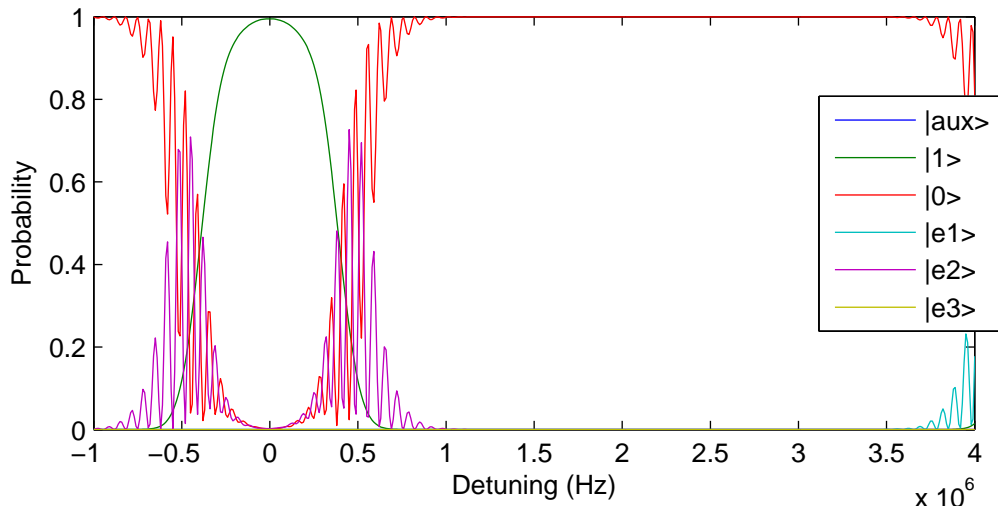
Figure 18: Probability to be in a certain state as a function of detuning for that ion. A NOT operation on one six level Pr ion with single-color pulses with pulse parameters from section 4.4
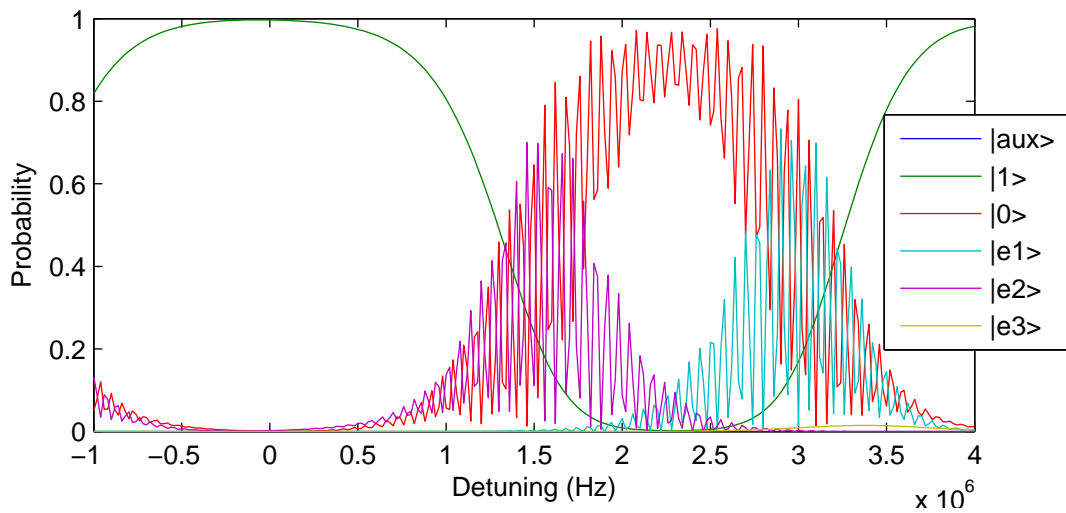
Figure 19: Probability to be in a certain state as a function of detuning for that ion. A NOT operation with single-color pulses with parameters in section 5.2.1 on a Pr ion

31
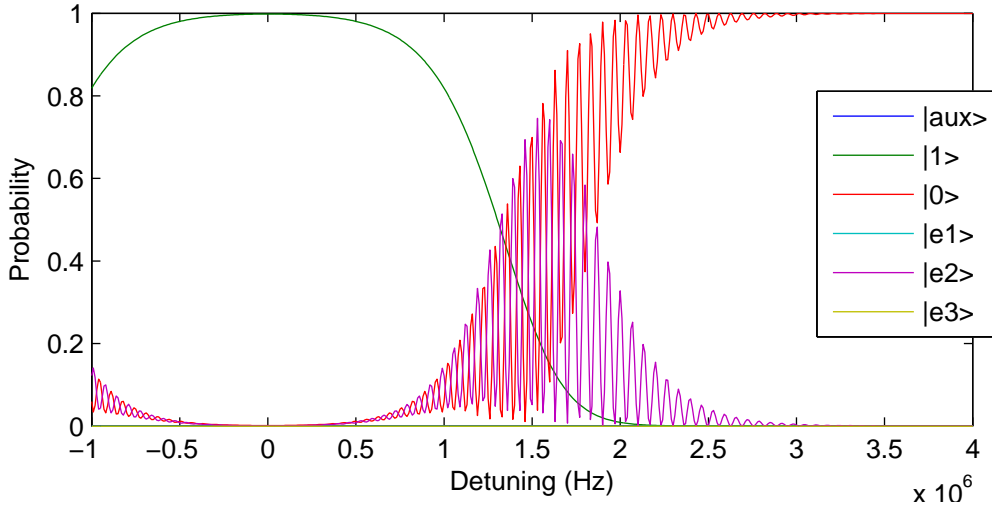
Figure 20: Probability to be in a certain state as a function of detuning for that ion. A NOT operation on a Eu ion with single-color pulses with parameters from section 5.2.1

the detuning dependent phase the first two pulses acquired.

As the operations are done in a crystal with lots of other ions with different resonance frequencies the change in probability as a function of the detuning from the laser frequency is very interesting. The ideal case would be that only the targeted ion is affected and none else, and thus a pulse with the frequency width equal to the homogeneous broadening would be wished for. However, remembering Heisenberg the pulse that is more narrow in frequency is longer in time and if the operation takes long time compared to the life time of the state the assumption that no dephasing occurs does not hold. Using the pulse parameters as mentioned, the model was expanded including all six levels that are close to each other and the two-color NOT operation was done. The end result as a function of the detuning is plotted in figure 23 and in figure 24 for Eu with figure 24 being a close-up around the resonance frequency.

The same was done for a Pr ion also with six levels in figure 25 and in figure 26. Especially for Pr is it notably how far from the ideal case it is. Because of the hyperfine splitting structure being much more closely spaced in energy than for Eu, the Raman transition terms for the other levels will interfere with the resonance transition terms.

5.2.3 Raman effect

To compare the full model with just the adiabatic model described in section 4.5 to see how big influence the adiabatic Raman transition have and to compare the two models, the operator presented there is used together with a two-color sechyp pulse with the parameters $\Omega_0 = 5*2\pi\text{Rad/s}$, $\beta = 1.7\text{MHz}$ and $\mu = 2.69$. Note that this single two-color pulse only results in taking the bright state to the excited level. Using the full model with a three level Eu ion result in figure 27. For Eu the splitting between the two ground levels is 90MHz which can
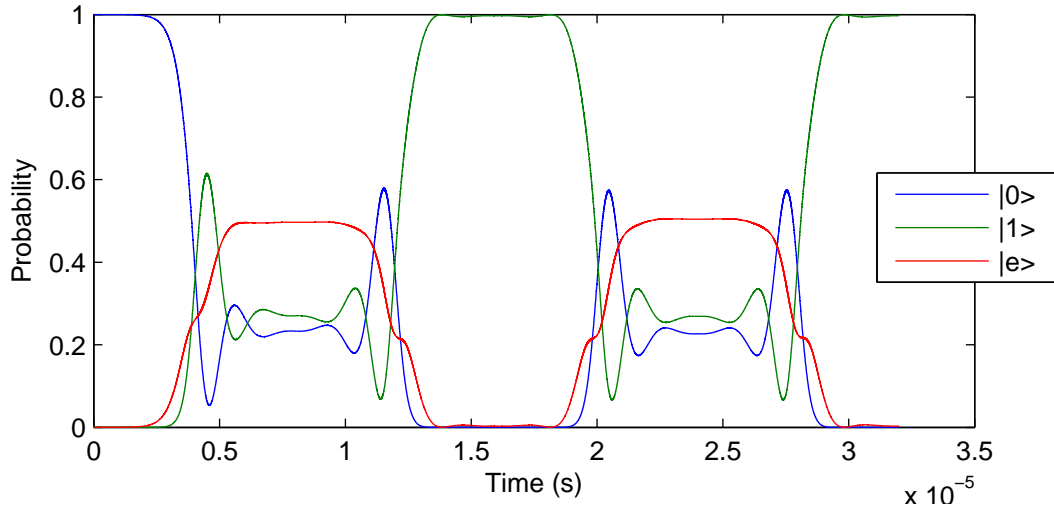
Figure 21: Probability to be in a certain state as a function of time. The change in population for an ion with zero detuning from light frequency being exposed to a NOT operation with two-color pulses
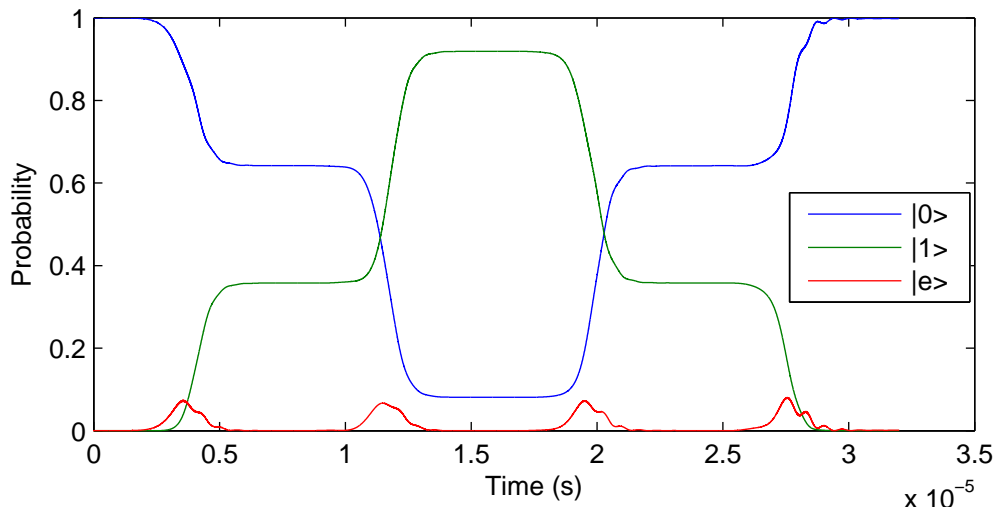
Figure 22: Probability to be in a certain state as a function of time. An Eu ion detuned with 1MHz from the light frequency and how the population changes as a NOT operation with two-color pulses are done and the compensation pulses brings the fidelity to one since a detuned ion should not be affected by the pulse
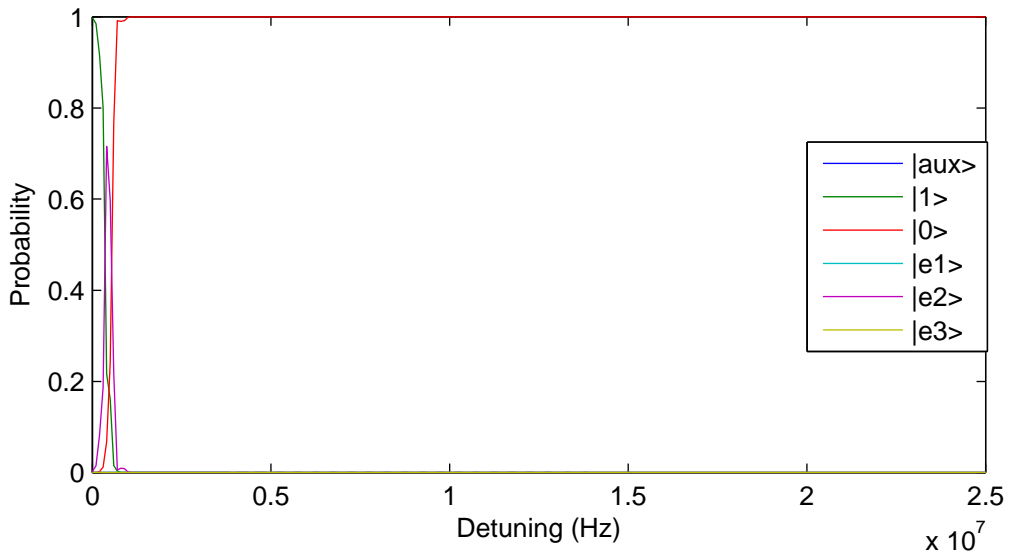
Figure 23: Probability to be in a certain state as a function of detuning for that ion. The end result after a NOT operation on a three level Eu ion with two-color pulses as a function of detuning from light frequency
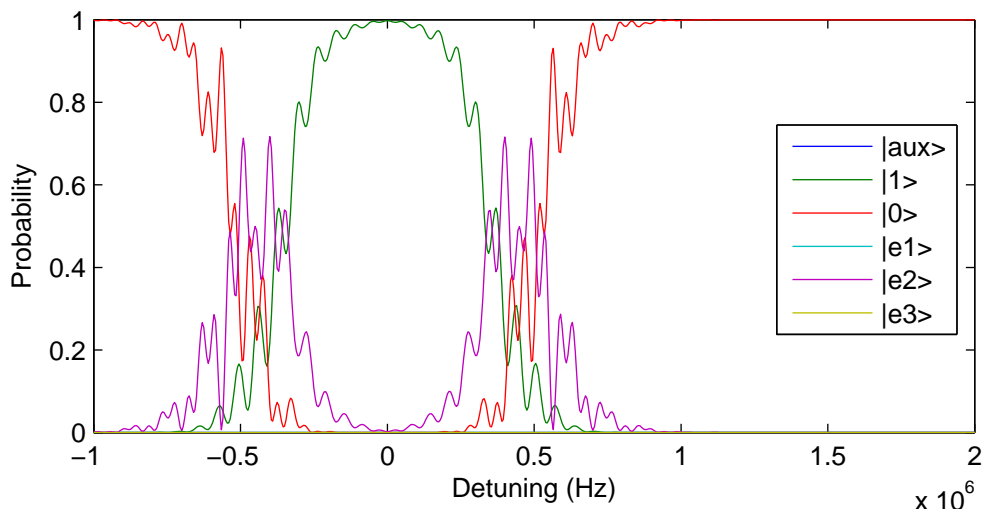
Figure 24: Probability to be in a certain state as a function of detuning for that ion. The same operation as for figure 23 but focused on small detuning
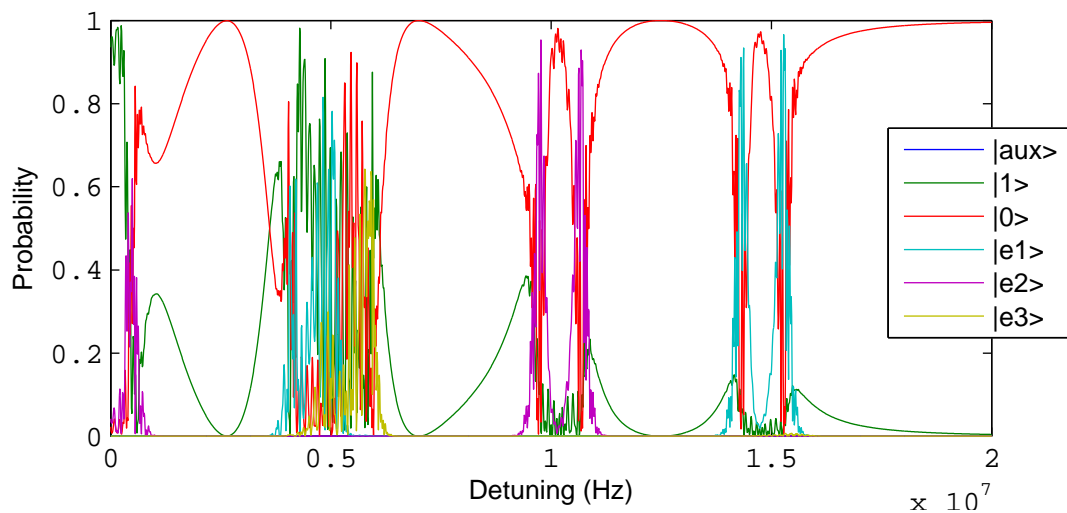
Figure 25: Probability to be in a certain state as a function of detuning for that ion. A NOT operation with two-color pulses is simulated for one Pr ion with six levels as a function of the detuning from the laser frequency.
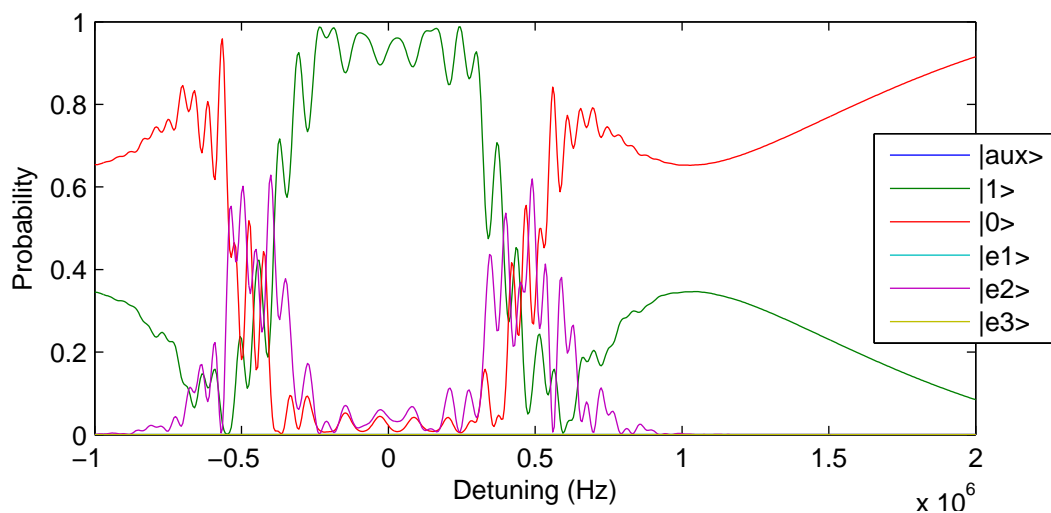
Figure 26: Probability to be in a certain state as a function of detuning for that ion. The same operation as for figure 25 but for frequencies close to zero detuning.

clearly be seen in the figure. Solving the same setup with the same pulse but using the adiabatic Raman model described in section 4.5 result in figure 28. The two figures are very similar except around 90MHz detuning where processes other than Raman transitions are expected to happen. Thus is seen that due to Raman transitions are even ions that are far detuned, on the order of 100MHz, affected by the pulse. This is an unwanted property of the pulse which makes it very difficult to target only one ion and in practice makes it impossible to use this pulse. Given that the two different approaches give similar result another conclusion is that the full model,the time evolution program, seems to give correct results.
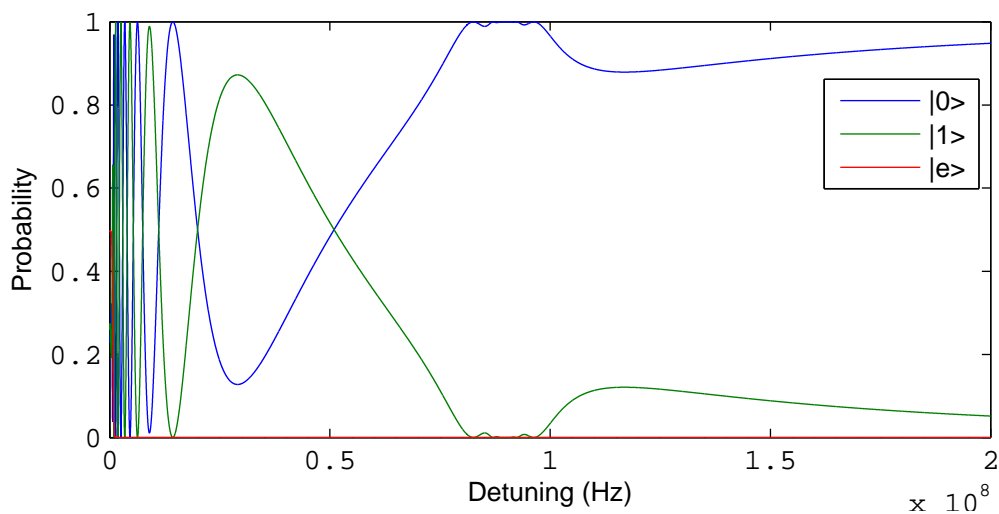
Figure 27: Probability to be in a certain state as a function of detuning for that ion. The end result in a simulation using one two-color pulse with $\Omega_0 = 5 * 2\pi\text{Rad/s}$, $\beta = 1.7\text{MHz}$ and $\mu = 2.69$

The Raman transitions depend strongly on the Rabi frequency. In figure 29 the pulse parameters used in section 4.4, most notably the $\Omega_0 = 0.55 * 2\pi\text{Rad/s}$ (i.e. almost an order of magnitude weaker than in figure 27), was used showing a significant change in how far detuned Raman transitions occurs, only a couple of MHz. Using pulses with lower Rabi frequencies can thus enable the use of two-color pulses when targeting one ion. Also the influence from the adiabatic Raman transitions for small detuning is weak as seen in the large difference between the two models. When the pulse is on resonance the contribution from the adiabatic Raman transition is indeed expected to be zero. However, for detunings larger than 1MHz the results from the two approaches agree and the contribution from Raman transitions are strong.

For single ion dynamics, single-color sechyp pulses have an ideal effect while two-color pulses introduce two photon processes which increase the number of unwanted ions that are affected by the pulse. However, as seen in figure 22 is some of the effect nullified with compensation pulses.
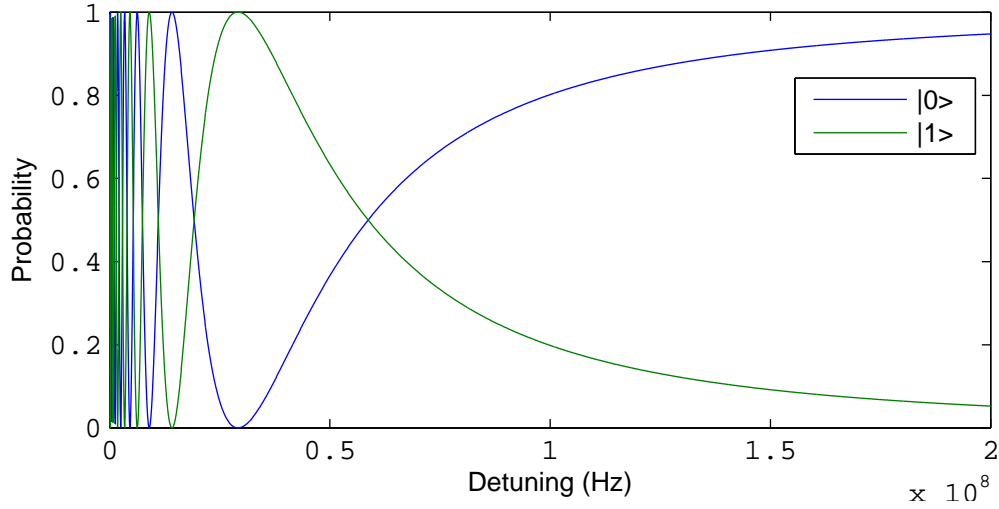
Figure 28: Probability to be in a certain state as a function of detuning for that ion. The end result after one two-color sechyp pulse with $\Omega_0 = 5 * 2\pi\text{Rad/s}$, $\beta = 1.7\text{MHz}$ and $\mu = 2.69$ using the adiabatic Raman transition model.
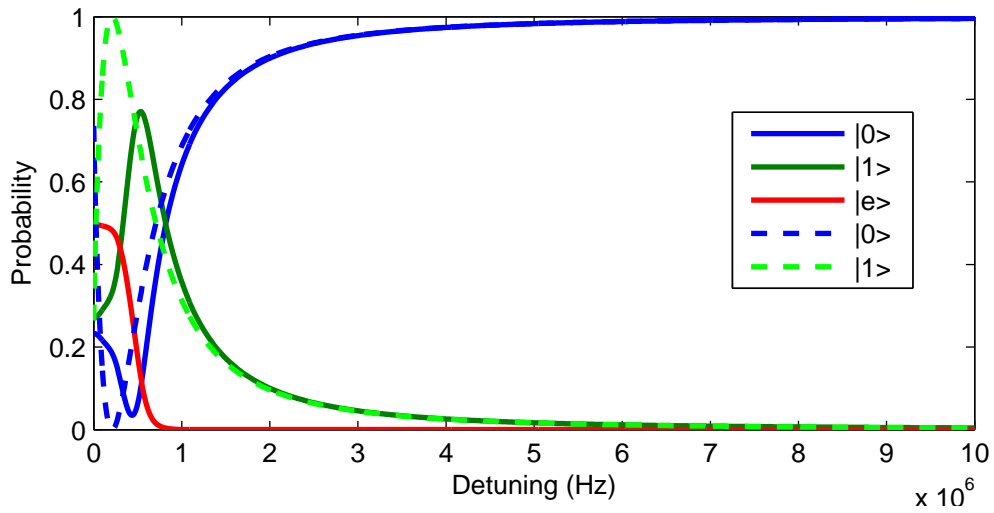
Figure 29: Probability to be in a certain state as a function of detuning for that ion. The adiabatic Raman solution for one two-color sechyp pulse with parameters in section 4.4 with $\Omega_0 = 0.55\text{MHz}$ (dashed line) and the simulated result with the same pulse parameters (solid line)

37

5.3 Multiple qubit dynamics

5.3.1 Multiple excitation from one pulse

Expanding the simulation to include two ions the effect of the interaction between them come into play. A single-color sechyp pulse was targeted at the resonance frequency of one ion and the wanted result is an excitation of that first ion and no change in the population for any other ion. Thus, in figure 30 the state $|e0\rangle$ is displayed as a function of detuning and dipole-dipole interaction between the target ion and the other ion. Both ions have six levels and the target ion is the one changing in frequency. First, for small detuning the second ion is affected by the pulse as well, resulting in loss in fidelity as seen in figure. Second the most prominent feature is the big valley, where the detuning between the ions roughly equals the shift in energy. This can be understood in the following way: as the target ion is excited the second ion is, due to dipole-dipole interaction, shifted to resonance with the target ion excitation frequency. It will then be picked up by the sechyp pulse and driven up to the excited state. The width of the rift is depending on how broad the sechyp is in frequency, and the spacing between the levels.
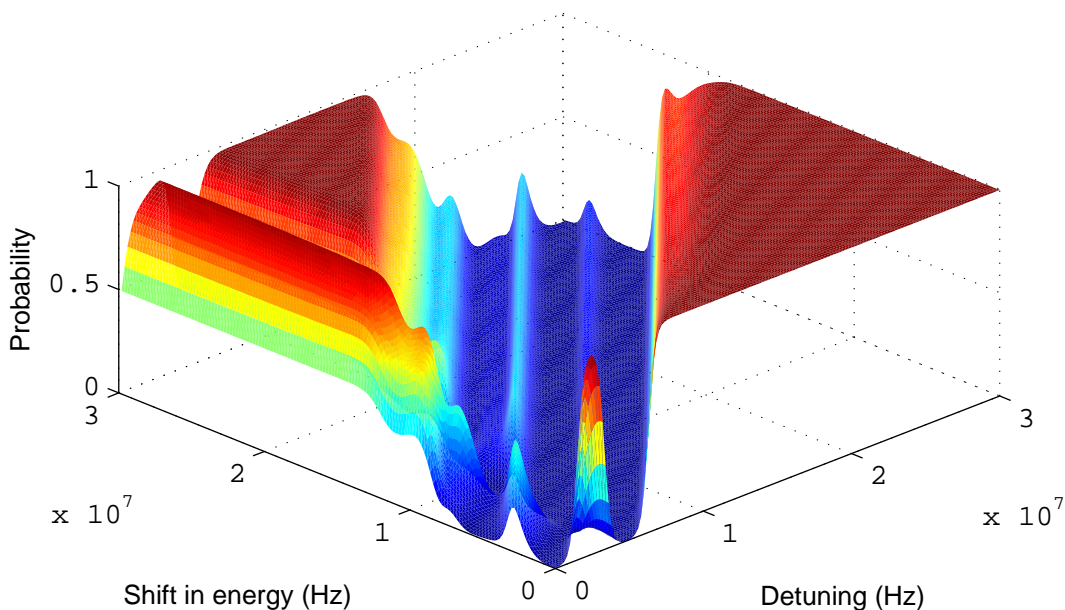
Figure 30: Probability to be in $|e0\rangle$ after a sechyp pulse with the parameters given in figure 28 as a function of detuning between the target ion and another ion and the shift in energy due to dipole-dipole interaction between them.

5.3.2 Simple pulse sequence

To know if the system works for gate operations, a system of three ions is set up with the resonance frequency of the second ion being 20MHz higher than

the first and the third being 20MHz higher than the second. They all shift each other 150MHz when excited. Applying a chain of sechyp pulses to this system, targeting the different ions, figure 32 shows the evolution in time of the system. The pulses are given with 8μs interval following the scheme in figure 31. With the first two pulses a blockade is attempted, i.e. if the excitation of the first ion can block the excitation of the second. As can be seen, there is no change in the probabilities around 12μs which is the center for the second pulse which shows that the blockade is successfull. The first ion is then retuned to the ground state by pulse 3. The second part, pulse 4 to 6, aims at changing the third ion from $|0\rangle$ to $|1\rangle$ and doing the excitation of the second ion, to show that a NOT operation is possible and that an ion in state $|1\rangle$ does not block the excitations.
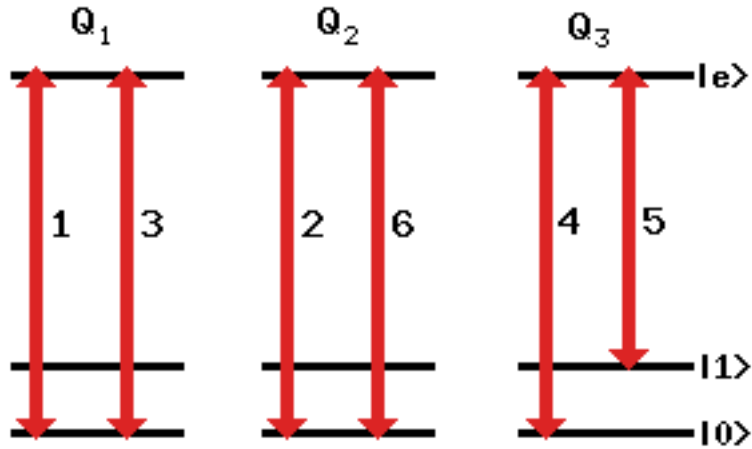
Figure 31: The scheme showing in which order and which energy the pulses were sent in

For the operations done in figure 32 the pulses were cut after 8μs and then followed by next. This way of giving the pulses causes loss in fidelity when shortening the times more than 2.5μs for each pulse as can be seen in figure 33. Another approach is to mix the energy fields from the different pulses and letting them continue for the whole duration of the operation. Doing so for these pulses and varying the time from center of one pulse to the center of next and noticing the probability at the end, figure 34 was acquired. Comparing these two results the mixing of the energy fields allow shorter time between the center of the pulses while keeping a high fidelity. Using this method with the system of three ions set up above and a center to center time of 1.6μs for the pulses, the result shared in figure 35 was obtained. As seen is the end result still the same with a high fidelity.

5.3.3 Deutsch-Jozsa algorithm

Extending the previous results a simulation of a real algorithm with many gate operations on a system of three ions was made, now without mixing the energy fields. The algorithm chosen was the Deutsch-Jozsa algorithm (see section 2.1)
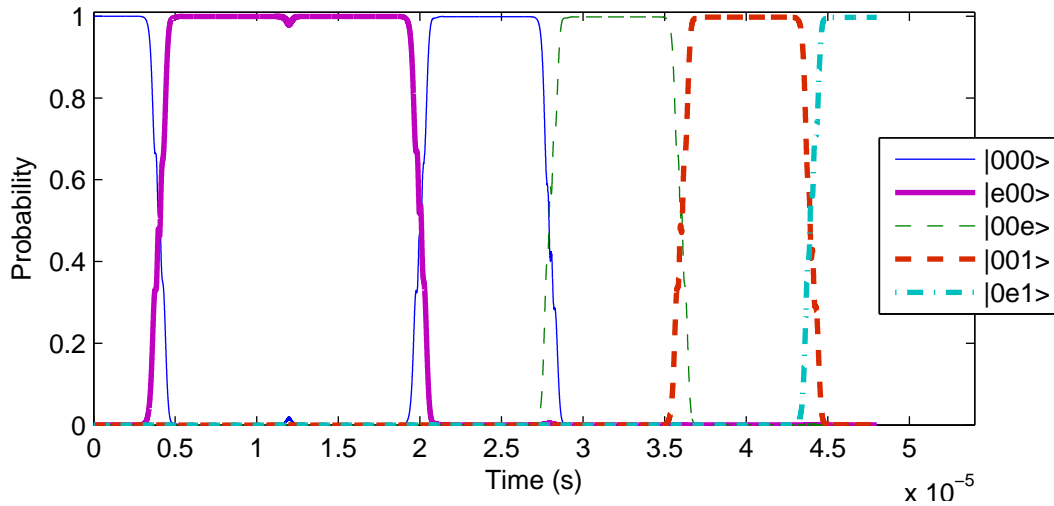
Figure 32: Probability to be in a certain state as a function of time. In a system of three ions with three levels sechyp pulses with parameters as in figure 28 are sent in following order: $Q_1 : |0\rangle \rightarrow |e\rangle$, $Q_2 : |0\rangle \rightarrow |e\rangle$, $Q_1 : |e\rangle \rightarrow |0\rangle$, $Q_3 : |0\rangle \rightarrow |e\rangle$, $Q_3 : |e\rangle \rightarrow |1\rangle$, $Q_2 : |0\rangle \rightarrow |e\rangle$ as seen in figure 31
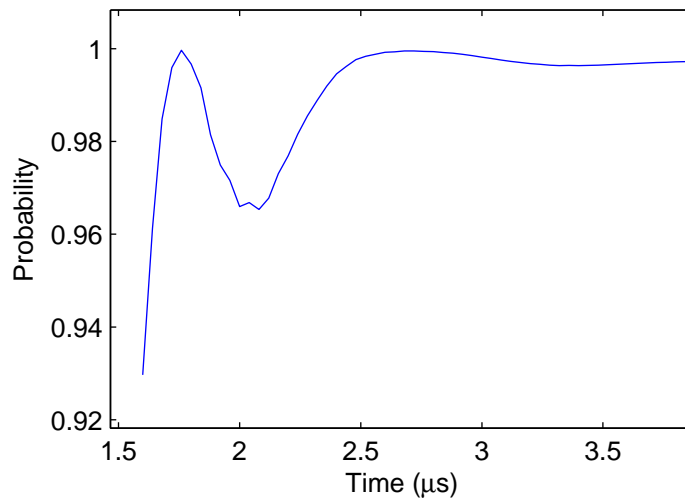
Figure 33: Probability to be in $|0e1\rangle$ after the operation in figure 32 as a function of the time between the center of the pulses when cutting each pulse as the next pulse is sent in
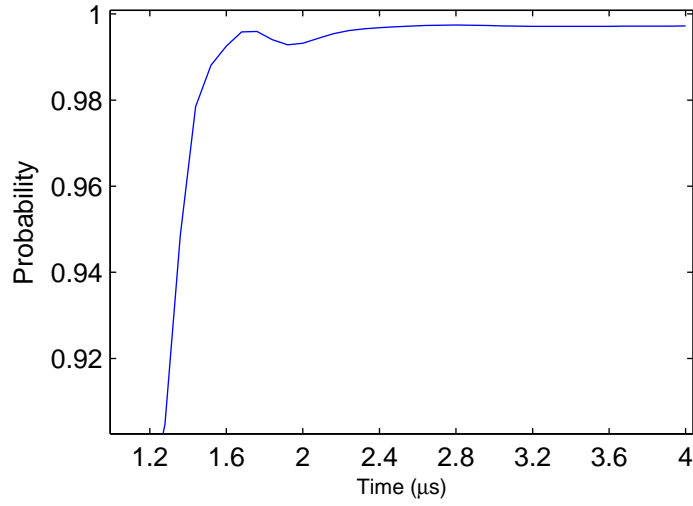
Figure 34: Probability to be in $|0e1\rangle$ at the end of the operations in figure 32 as a function of time between pulse centers for overlapping pulses
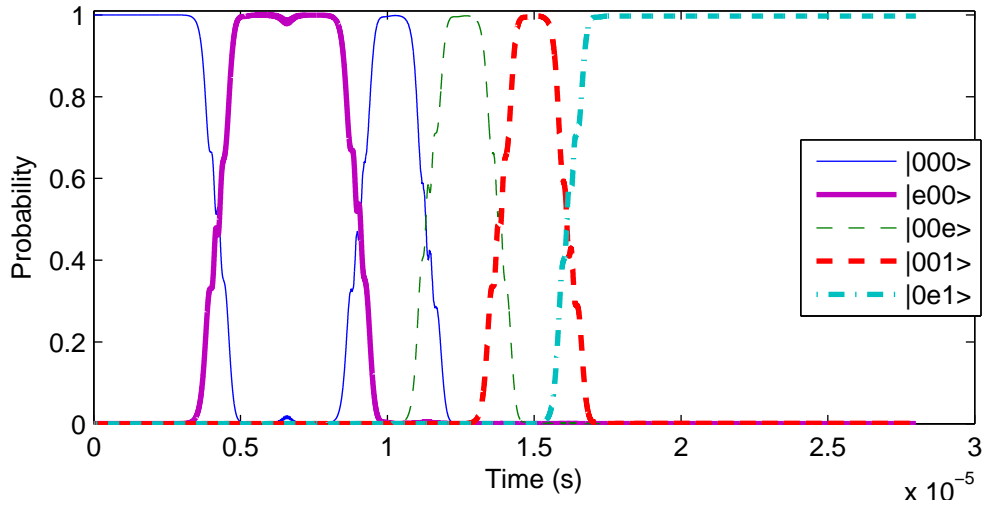
Figure 35: Probability to be in a certain state as a function of time. The same pulse scheme as for figure 32 but with the energy fields mixed together with $1.6\mu s$ between the center of the pulses

for a query register of two qubits with the third being the qubit in an answer register. The initial state of the system has the query register qubits in $|0\rangle$ and the answer register qubit in $|1\rangle$. To realize the Hadamard gates two-color pulses were used which, since it is two rotations, require 8 pulses and the function chosen was a CNOT which is a balanced function. The qubits were chosen with the second qubit being 40MHz detuned from the first and the third being 170MHz detuned from the first. Excitation of any ion shift the resonance frequencies of the other two ions 300MHz, via the dipole-dipole interaction, and the evolution in time for the system can be seen in figure 36. In the figure the system starts in the initial state $|001\rangle$ and three Hadamard gates are applied, one per qubit. After little less than 200μs the function is applied and to finish of is a Hadamard gate applied to the first and second qubit. When measuring the state of the first qubit there is a higher than 95% probability to find it in state $|0\rangle$ and the same high probability is it to find the second qubit in state $|1\rangle$ when measuring. Thus the probability is very high to get the result that the function is balanced!
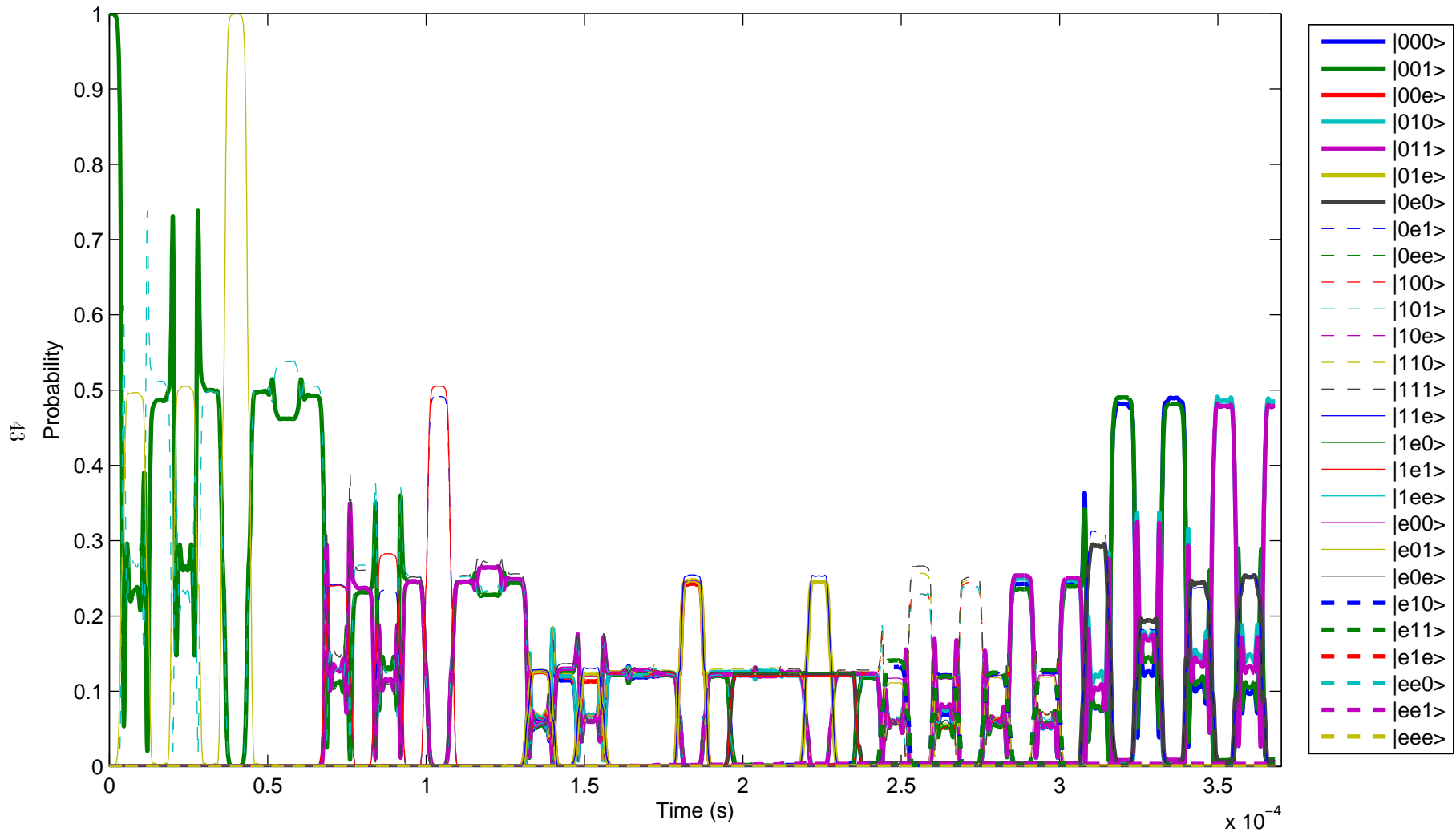
Figure 36: Probability to be in a certain state as a function of time. A Deutsch-Jozsa algorithm was made with two qubits in the query register. The function is a CNOT operation and thus balanced and should return 1 in one of the query register qubits at the end. After setting up the system with three Hadamard gates the function is applied and then two Hadamard gates are applied to Q_1 and Q_2 and the output is that Q_2 has a high probability to be in state 1 and the function is thus balanced

To sum this part up, increasing the number of ions in the simulation expands the problems many times and in different direction, both becoming more time consuming and introducing shifts from interactions with all the other ions. Still a small quantum algorithm was successfully simulated.

5.4   Qubit chain statistics

Connecting the two approaches to quantum computing, the modeling approach and the simulating approach, would be to send in pulses to the ions in a crystal and use the interaction between them and their frequencies. A step in that direction is to pick out the ions from a realization that can be a part of a quantum operation chain. Between two qubits the criteria is that the frequencies should not overlap so that targeting one ion will affect the other ion, neglecting the shift in resonance frequency due to dipole-dipole interaction. Using Pr ions and giving each a frequency channel with at least 20MHz to another ions resonance frequency in the chain, a number of chains can be constructed starting from the ions that shift the read-out ion more than 30MHz. The chain containing most ions is marked in the realization in figure 37 with green halos and the ions that shift the read-out ion enough have a green line drawn.

With an increase in doping concentration the interactions between the ions in the crystal are stronger and more numerous. Consequently the change in the size of the chain as a function of the concentration is interesting. The average size of 50 realizations is seen in figure 38 and except for small doping concentrations the increase is linear. To understand this development it must be remembered that the inhomogeneous broadening increase linearly with the doping concentration (section 3.7). Still, it could be that the length of the largest chain changes very much between different realization but that is not the case as can be seen in figure 39. Thus, at a certain doping concentration the probability to find a chain where most channels are occupied will be high and so the limiting parameter is the width of the inhomogeneous broadening.
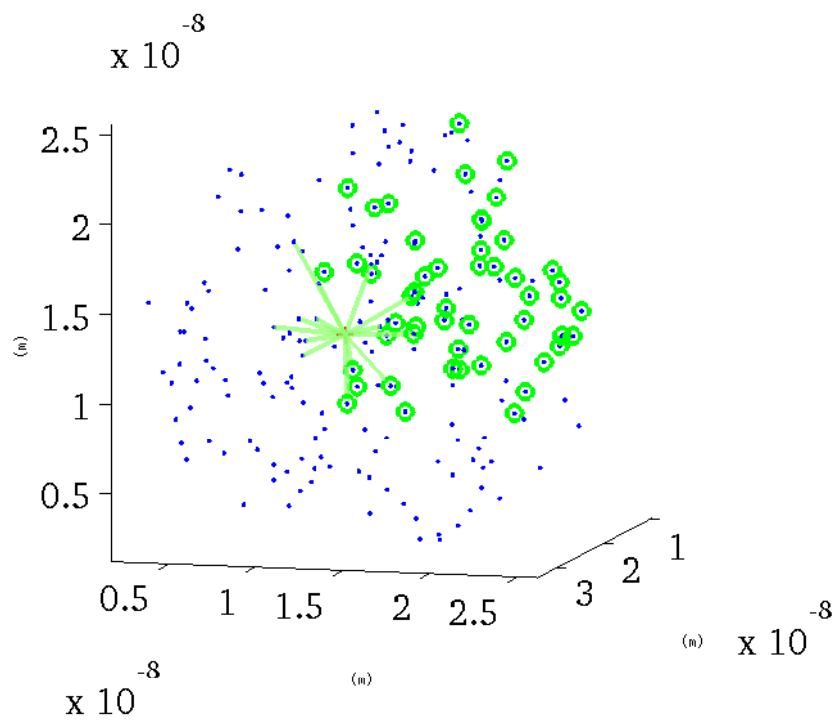
Figure 37: The model of the crystal doped with 0.2% Pr with the read-out Ce ion in the middle with green connections to all ions that shift it more than 30 MHz. The biggest chain where there are not two ions within 20MHz from each other in resonance frequency is made up of the ions with a green halo
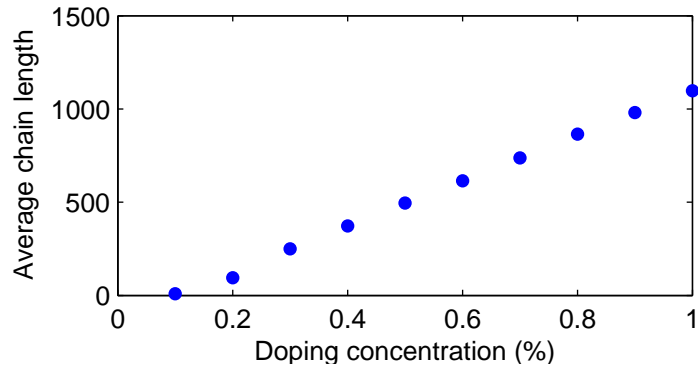
Figure 38: The average of numbers in the biggest chain out of 50 realizations as a function of different doping concentrations.
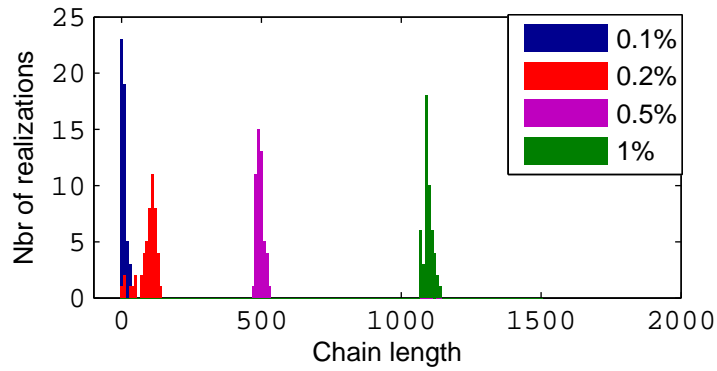
Figure 39: The distribution of the length of the biggest chain for four doping concentrations with 50 realizations each.

6   Conclusions

To conclude, a high fidelity of the operations is wanted and the pulses result in a target frequency range of the order of 100kHz for high fidelity, which means that the number of ions close by should be as low as possible to minimize shifts on the target ion. This gives that the doping concentration should be as low as possible. At the same time a chain of ions that can be used for operations should be formed with a high certainty to simplify the practical search for a working quantum system. From figure 39 this gives for Pr a higher doping concentration than 0.2%.

When using two-color pulses the pulse parameters with lower Rabi frequency are better for minimizing excitations of other ions in the system due to Raman transitions. For single color pulses a higher frequency chirp ($\beta*\mu$) value is better since there is a trade-off between not exciting other ions and a robustness of the system which drives the operation with high fidelity, even if the target ion is shifted a bit.

Between the two ions Eu is preferable since the fidelity for two-color pulses is higher. This will be a bit trickier since the larger hyperfine splitting result in simultaneous excitation frequencies at around 100MHz away from the resonance frequency. The mapping of a functioning chain will thus be problematic but at the same time other ions that have resonance frequencies in between the target ion excitation frequencies can be allowed.

7   Acknowledgements

References

[1] L. ALLER AND J. H. EBERLY, *Optical resonance and two-level atoms*, Dover publications, Inc., 1975.

[2] X. CAILLET AND C. SIMON, *Precision of single-qubit gates based on raman transitions*, Eur. Phys. J. D, 42 (2007), pp. 341–348.

[3] F. R. GRAF, A. RENN, AND U. P. WILD, *Site interference in stark-modulated photon echoes*, Physical Review B, 55 (1997), pp. 11225–11229.

[4] F. R. GRAF, A. RENN, G. ZUMOFEN, AND U. P. WILD, *Photon-echo attenuation by dynamical processes in rare-earth-ion-doped crystals*, Physical Review B, 58 (1997), pp. 5462–5478.

[5] J. JACKSON, *Classical Electrodynamics, 3rd ed.*, John Wiley & Sons, Inc., 1998.

[6] R. KOLESOV, K. XIA, R. REUTER, R. STÖHR, A. ZAPPE, J. MEIJER, P. HEMMER, AND J. WRACHTRUP, *Optical detection of a single rare-earth ion in a crystal*. Submitted to Nature photonics, april 2012.

[7] F. KÖNZ, Y. SUN, C. THIEL, AND R. CONE, *Temperature and concentration dependence of optical dephasing, spectral-hole lifetime, and anisotropic absorption in $Eu^{3+} : Y_2SiO_5$*, Physical Review B, 68 (2003).

[8] G. LIU AND B. JACQUIER, eds., *Spectroscopic properties of rare earths in optical materials*, Springer, 2005, ch. 7.

[9] B. LUO, S. KRÖLL, R. EQVALL, Y. SUN, F. KÖNZ, AND R. CONE, *Dephasing processes induced by ion-ion interactions in $Pr^{3+} : Y_2SiO_5$*. Unpublished, Dec 2002.

[10] B. MAKSIMOV, V. ILYUKHIN, Y. KHARITONOV, AND N. BELOV, *Crystal structure of yttrium oxyorthosilicate $Y_2O_3 \cdot SiO_2 = Y_2SiO_5$. dual function of yttrium*, Soviet Physics - Crystallography, 15 (1971), pp. 806–812.

[11] M. NILSSON, *Coherent interactions in rare+earth+ion+doped crystals for applications in quantum information science*, PhD thesis, Lund University, Department of physics, 2004.

[12] L. RIPPE, *Quantum computing with naturally trapped sub-nanometre-spaced ions*, PhD thesis, Lund University, Department of physics, 2006.

[13] ——, *Single qubit preparation and tomography with two-colour complex hyperbolic secant pulses*. Internal notes, Quantum information group, Lund University, 2006.

[14] M. O. SCULLY AND M. S. ZUBAIRY, *Quantum optics*, Cambridge university press, 1997, ch. 7.

[15] M. SELLARS, E. FRAVAL, AND J. LONGDELL, *Investigation of static electric dipole-dipole coupling induced optical inhomogeneous broadening in $Eu^{3+} : Y_2SiO_5$*, Journal of Luminescence, 107 (2004), pp. 150–154.

[16] K. TORDRUP, *Quantum computing in ensamble systems*, PhD thesis, University of Aarhus, LTC, 2008.

[17] R. YANO, M. MITSUNAGA, AND N. UESUGI, *Ultralong optical dephasing time in $Eu^{3+} : Y_2SiO_5$*, Optics Letters, 16 (1991), pp. 1884–1886.